

## **Features of locally and remotely generated surface gravity waves in the inner-shelf region of north-western Bay of Bengal**

M. Anjali Nair, V. Sanil Kumar\*, M.M. Amrutha, V.S.N.Murty

Ocean Engineering Division, CSIR-National Institute of Oceanography (Council of Scientific & Industrial Research), Dona Paula-403 004, Goa, India

\*corresponding author Tel: 0091 832 2450 327 Fax: 0091 832 2450 602

email:sanil@nio.org URL: www.nio.org

### **Abstract**

In this article, we studied the characteristics of locally and remotely generated wind-waves in the inner-shelf region of north-western Bay of Bengal (BoB) based on the measured wave data. Two well-differentiated wave systems, one young sea from the east-southeast and another more developed swell from the south lead to bimodality in the wave spectrum. Wind-sea predominance is not observed in the monthly average wave spectrum and in all the months swells dominated indicating a swell-driven wave regime. During the monsoon (JJAS), the wave climate is dominated by long-period swell from the south-southeast and the short fetch during the northeast monsoon (ONDJ) leads to weaker easterly swells, while the effects of the sea/land breeze influence on the wave generation are more relevant during this season. During November-April, diurnal variation of 0.15 m in significant wave height (SWH) is observed. This study based on seasonally averaged ERA-Interim reanalysis data reveals a weak connection between the waves in the northwestern BoB and the El Niño Southern Oscillation (ENSO) and Indian Ocean Dipole (IOD) events. The waves are influenced by ENSO events during June-September and by IOD events during October-January, which consequently caused inter-annual variations in monthly average SWH. The present study, however, did not show a significant inter-annual variability in annual mean SWH during 1979-2015.

**Index Terms:** Oceans, Regional climate change, ocean sciences, decadal ocean variability, surface waves and tides

**Keywords:** Surface waves, mixed sea state, ocean science, wind-seas, multi-peaked spectra, swells, Indian wave climate

## 1. Introduction

The ocean surface waves or wind-waves generated by winds are of importance for scientific and industrial applications (Kinsman, 1965). In the ocean, waves generated at different regions by different meteorological events propagate and reach at a particular location (Portilla et al., 2015). Generally, the wind-sea (waves influenced by the local wind) and swells (waves that are away from the generating area and no longer affected by the local wind) co-exist at a location (Hanson and Phillips, 2001; Hanley et al., 2010). When the waves propagate from deep water to intermediate/shallow water depth, they interact with the sea bottom and keep the bed sediments in suspension. These suspended sediments are moved by the nearshore currents. The surf-zone, inner-shelf (~5 to 15m water depth) and mid-shelf (~15 to 50m water depth) represent the transition area from land to the open ocean. The Visakhapatnam City beach situated along the east coast of India (Figs. 1 and 2), is undergoing erosion. Sand bypassing is being carried out to reduce the erosion of the beach. The wave is one of the important parameters responsible for the erosion of the beaches (Kinsman, 1965). Longshore currents and rip currents are formed in the nearshore regions due to the radiation stresses generated by the waves (Longuet-Higgins and Stewart, 1964) and they control the littoral drift pattern. The wave-driven redistribution of beach nourishment sand is an important component of the complex cost-benefit analysis of the beach nourishment project and is poorly understood (Ludka et al., 2016). Hence, it is important to understand the wave characteristics during different seasons and its inter-annual variations before planning the coastal protection measures.

The Bay of Bengal (BoB) is one of the largest semi-enclosed basins in the northern hemisphere and is part of the North Indian Ocean (Fig. 1). Observational wave data in the BoB are sparse. Only few wave buoy records exist and these are intermittent (Sanil Kumar et al., 2001; Suresh et al., 2010; Johnson et al., 2013; Amrutha et al., 2014; Sanil Kumar et al., 2014; Patra et al., 2016). Sanil Kumar et al. (2014) reported that the seasonal average value of significant wave height (SWH) varied from 0.8 m in the northeast (NE) monsoon season (ONDJ) to 1.3 m in the SW monsoon (JJAS) season along the north-western BoB. In the North Indian Ocean (NIO) relatively weaker winds and waves are observed in the boreal winter (ONDJ) (Anoop et al., 2015). Whereas, BoB is the region where the deadliest tropical cyclones (generally referred to as a hurricane in the Atlantic and the Eastern Pacific and a typhoon in the Western Pacific) occurred (Balaguru et al., 2014). During the tropical cyclone (TC), high waves with SWH of ~6 to 8 m were measured in the BoB (Amrutha et al., 2014). The occurrence of TCs in BoB is high in May and in October-November, indicating an annual bimodal structure (Balaguru et al., 2014). In the BoB, the winds reverse their direction between the SW monsoon and NE monsoon (Fig. 3) and the seasonal average

wind speed is high (~8-10m/s) during the SW monsoon (Fig. 3b) and is low (~4-6 m/s) during the remaining period (Fig. 3a,c). Due to the seasonally reversing winds, the waves also show seasonal behaviour (Sanil Kumar et al., 2014).

Earlier studies indicate that the waves in the north-western BoB consist of wind-seas and swells with the predominance of swells (Sanil Kumar et al., 2014; Patra et al., 2016). In most of these studies, integrated wave parameters of the spectrum are considered (Sanil Kumar et al., 2001; Suresh et al., 2010; Patra et al., 2016). In the case of uni-modal seas, the bulk wave parameters give a good indication on wave characteristics, but in more complex situations like the simultaneous existence of wind-seas and one or more swells, using only integrated parameters is often insufficient and misleading (Sanil Kumar et al., 2001; Portilla et al., 2015). The co-existence of wind-seas and swells from different directions significantly affect the direction of littoral drift (Sanil Kumar et al., 2001). For a complete description of the sea state, the wave spectral characteristics have to be studied in detail and the different wave systems present at a location are to be isolated.

The variability in wave climate has different time scales, ranging from hour, day, month, season, year and decade (Anoop et al., 2015). To study the changes in wave height over the years, we choose ERA-Interim reanalysis data (Dee et al., 2011) more than 30yr, consistent with the period used by most weather and climate studies (Hansen et al., 2012). Generally the wave data at a location is based on i) ship-based visual observations (Gulev and Grigorieva, 2004), ii) altimeter data (Young et al., 2011), iii) numerical modelling (Semedo et al., 2011), and iv) buoy measurements or combination of one or two of these (Anoop et al., 2015). Shanas and Sanil Kumar (2015) observed that in the central BoB, ERA-Interim SWH compared well with buoy measured data for mean values and they also observed significant deviation during high waves (SWH >2.5m).

Large-scale patterns of oceanic variability on longer timescales can be explained by teleconnections at Global scale. The El Niño Southern Oscillation (ENSO) is the major source of inter-annual climate variability (Philander, 1990) and its signatures are observed as the temperature fluctuations in surface waters of the tropical Eastern Pacific Ocean. The main regional symptoms of ENSO are the increase in sea surface temperature (SST) and the reduction of wind speeds (Wyrki, 1981). The Indian Ocean Dipole (IOD) is the coupled oceanic and atmospheric phenomenon in the equatorial Indian Ocean similar to the ENSO (Saji et al., 1999). The inter-annual variability of extreme wave heights in the world ocean is influenced by large-scale teleconnection patterns, such as ENSO, Southern Annular Mode (SAM) or Antarctic Oscillation (AO) (Izaguirre et al., 2011). It is shown that the waves in the northern hemisphere are affected by modes like North Atlantic Oscillation (NAO) and Arctic Oscillation (Semedo et al., 2015; Liu et al., 2016). During the positive

phase of the NAO, larger waves are observed at northern latitudes of the Atlantic coast of Europe. Studies in the southwest (SW) Pacific along the Australian shelf based on wave buoy observations indicates that ENSO significantly modulates wave climate (Harley et al., 2010). In the Indian Ocean, Lopez and Kirtman (2016) observed a nonlinear influence of the ENSO on large wave height events. The above studies show that wave heights of different regions of world ocean are correlated with climate indices; i) NAO (Dodet et al., 2010), ii) SAM (Hemer et al., 2010), iii) ENSO (Gulev and Grigorieva, 2004; Hemer et al., 2010; Lopez and Kirtman, 2016) and iv) IOD (Anoop et al., 2016). The two modes, namely ENSO and IOD, are patterns which have significant impacts on winds in the Indian Ocean (Girishkumar and Ravichandran, 2012). Since ENSO and IOD events manifest most strongly during late boreal fall and early winter (October-November), they influence the post-monsoon winds over the BoB (Balaguru et al., 2014). In the south-eastern BoB, Johnson et al. (2013) reported that the single-peaked wave spectra observed from waverider buoy during SW monsoon of 2011 coincide with the presence of positive IOD. Anoop et al. (2016) noted that the changes in the equatorial SST and sea level pressure due to IOD influenced the measured waves in the eastern Arabian Sea (AS). The influence of IOD and ENSO events on the wave climate of the north-western BoB is not yet examined.

In this present paper, we studied the characteristics of locally and remotely generated waves in the inner-shelf at a location off Visakhapatnam in the north-western BoB along with the spectral characteristics of waves. Our study is based on the measurements collected by a moored directional waverider buoy at 15m water depth for one year period. Since ENSO and IOD events influence winds over the Indian Ocean, we have examined the influence of IOD and ENSO events on the waves in deep water location (water depth~70m) based on ERA-Interim reanalysis data. The wave characteristics at Tikkavanipalem, a location 30 km south of Visakhapatnam during December 1997-November 1998 are studied based waves measured at 12 m water depth (Sanil Kumar et al., 2001). The wave spectral characteristics during 2010 off Gangavaram, 11 km south of the present study area are reported by Sanil Kumar et al. (2014). We have also compared the wave characteristics with that reported in Sanil Kumar et al. (2001) and Sanil Kumar et al. (2014). Based on the wave data collected during the SW monsoon of 2009, Suresh et al. (2010) studied the wind-seas and swells off Gangavaram and reported that waves are mainly swells during the SW monsoon.

## **2. Materials and methods**

Wave data measured at A (geographic location 17° 42.3'N, 83° 19.7'E) using the Datawell Directional Waverider buoy (Datawell, 2009) during 1 March 2015 - 29 February 2016 are used in the study. The area is exposed to waves from northeast to SW, and the nearest landmass is ~ 980km

in the northeast (Myanmar), ~ 1100km in the east to southeast (Myanmar and Andaman & Nicobar), ~ 9300km in the south (Antarctica) and ~ 500km in the SW (India) (Fig. 1). Hence, the swells from the Southern Ocean and the south Indian Ocean can reach the study area. The data recorded at 1.28Hz and the same for every 30 minutes are processed as one record. There are no data gaps and a total of 17,568 data records covering one-year period are analysed. From the measured heave data of the buoy, the wave spectrum is computed using Fast Fourier Transform (Datawell, 2009). As higher frequency measurements can introduce noise, all outputs of the buoy sensors are filtered by applying a low-pass filter with 0.58 Hz cut-off frequency. For frequencies less than 0.1Hz, the frequency resolution is 0.005 Hz and it is 0.01Hz for 0.1 to 0.58Hz. The details of the data collection and analysis are similar to that presented in Sanil Kumar et al. (2014). SWH and mean wave period ( $T_{m01}$ ) are obtained from the spectral moment. From the measured time series of vertical (heave) and the two horizontal translational motions of the buoy, mean wave direction ( $D_m$ ) is estimated based on circular moments (Kuik et al., 1988). The peak wave period ( $T_p$ ) corresponding to the peak frequency is obtained from the wave spectrum.

The directional spectrum of the surface wave field  $E(f, \theta)$  represents the density of the sea surface variance at each frequency ( $f$ ) and direction ( $\theta$ ). The SWH associated with particular

frequency and direction band is estimated as  $SWH_{s_1} = 4 \sqrt{\int_{f_1}^{f_2} \int_{\theta_1}^{\theta_2} E(f, \theta) df d\theta}$ . The 1-D separation

algorithm proposed by Portilla et al. (2009) is used to separate the wind-seas and swells based on the assumption that the energy at the peak frequency of a swell cannot be higher than the value of a Pierson-Moskowitz (PM) spectrum with the same frequency. If the ratio between the peak energy of a wave system and the energy of a PM spectrum at the same frequency is above a threshold value of 1, the system is considered to represent wind-sea, else it is taken to be swell. A separation frequency  $f_c$  is estimated following Portilla et al. (2009) and the SWH associated with swells ( $f_1 = 0.025$ ,  $f_2=f_c$ ) and wind-seas ( $f_1 = f_c$ ,  $f_2=0.58$ Hz) are separated and the waves from direction bands 0-44 & 244-360° (representing waves from the land direction i.e. the reflected waves and the waves generated due to land breeze), 44-136° (representing waves which cause south-westerly littoral drift) and 136-228° (representing waves which cause north-easterly littoral drift).

The contribution of long-period waves ( $T_p > 12$ s), intermediate ( $6 < T_p < 12$ s) and short-period waves ( $T_p < 6$ s) for the study area is also evaluated. The relationship between  $U/gT_p$  and  $U^2/gSWH$  as per equation (1) is used for analysing wind-sea/swell regimes (Hasselmann et al., 1976). Where,  $U$  is the wind speed and  $g$  is the acceleration due to gravity. Measurements are made

in Coordinated Universal Time (UTC) and the time reported in the paper is UTC. Standard meteorological convention of direction is used for winds and waves. From the wave spectrum measured at half-hourly interval, the monthly and seasonally averaged wave spectrum are computed by averaging the spectral energy density at the respective frequencies over the specified time.

$$\frac{U}{gT_p} = 4.8 \times 10^{-2} \left( \frac{U^2}{gSWH} \right)^{0.66} \quad (1)$$

The wave data measured at location B (17.632°N; 83.265°E) during the year 2010 (Sanil Kumar et al., 2014) and during October 2015 and at location C, a location 30 km south of Visakhapatnam (Fig. 2) during December 1997-November 1998 (Sanil Kumar et al., 2001) are used to compare the average wave characteristics observed in the present study. To study the inter-annual variations in wave height and the influence of IOD and ENSO events on waves, we used 37-yr (1979-2015) global atmospheric reanalysis dataset: ERA-Interim SWH (Dee et al., 2011) along with the 10-m wind speed data at 6-h temporal and 0.75° spatial resolution at 17.5° N, 83.5° E, which is the point from ERA-Interim dataset closest to the measurement location of Visakhapatnam. Wind pattern of the area for one year period (March 2015 to February 2016) is also studied. The correlation between different parameters is calculated using the statistical tools.

The comparison of ERA-Interim SWH with the measured buoy data shows a correlation coefficient of 0.90, bias of 0.14 m and root mean square error (RMSE) of 0.24m (Table 1). The comparison SWH is relatively better during February-May compared to other seasons, whereas the wave period has a better comparison during the SW monsoon. The time series of the measured and ERA-Interim SWH shows that the high waves (SWH >2m) are overestimated in ERA-Interim (Fig. 4a). The maximum SWH in the ERA-Interim data is 3.60 m and the annual average value is 1.22m, whereas the measured maximum SWH is 2.38 m and the annual average is 1.07m. The overestimation of the SWH and the large difference in the mean wave direction from ERA-Interim compared to the measured data (Fig. 4d) and is due to the fact that ERA-Interim data point (17.5°N, 83.5°E) is 29km away from the buoy location and is a deep water location (water depth ~70m), whereas the buoy measured data at 15 m water depth.

The strength of IOD and ENSO events are determined from SST anomalies of different regions and quantified as Dipole Mode Index (DMI), and Oceanic Niño Index (ONI). DMI is downloaded from the Japan Marine Science and Technology Centre website [www.jamstec.go.jp](http://www.jamstec.go.jp). ONI is from the National Oceanic and Atmospheric Administration ([www.cpc.ncep.noaa.gov/products/analysis\\_monitoring/ensostuff/ensoyears.shtml](http://www.cpc.ncep.noaa.gov/products/analysis_monitoring/ensostuff/ensoyears.shtml)). For revealing

the connection between large-scale atmospheric patterns and the waves, data separated into different seasons and correlation patterns between seasonally averaged ERA-Interim SWH data and climate indices is considered instead of the time series data for the whole year, since the waves in the study area are strongly affected by seasonal variability.

### **3. Results and discussions**

#### **3.1. Variations in bulk wave parameters**

The SWH oscillations in Fig. 4a reached the local maximum in June and exhibited greater values than the annual mean (~1m) during the SW monsoon months. During the SW monsoon, mean SWH (~1.4m) is larger than annual average and during the NE monsoon, mean SWH (~0.8m) is weaker than the annual average. In the study area, SW monsoon wave heights contribute 45% of the annual total wave heights (Fig. 5a). During the 1-year period, SWH varied from 0.5 to 1.5m for 78.8% of the time and is similar to the value (77.2%) reported at Gangavaram (location B which is ~11km SW of present measurement location) during 2010 (Sanil Kumar et al., 2014). The waves in this area tend to be smaller, so 51% of the SWH in an annual cycle is below 1m. Even though the measurements are done in different years and at different locations spanning 11km apart, the average SWH measured by the two buoys is very similar.

The SWH of monthly average wave spectrum is relatively high (1.56m) in July due to the SW monsoon influence and is minimum (0.60m) in January (Fig. 6a). SW monsoon influences both the AS and BoB. Hence, it is important to know the wave characteristics in both the western BoB and the eastern AS. The maximum monthly average SWH in the study area (1.56m) is less than the value (1.84m) observed in the eastern AS (Honnavar) during the same period (Fig. 6a). In the eastern AS, the annual maximum monthly average SWH is 2.1m and is observed in June (Sanil Kumar and George, 2016), whereas the corresponding value for the study area in June is 1.48 m. In November, the monthly average SWH is 1.1m in the study area, whereas it is 0.5m in the eastern AS. The annual average SWH of the study area (~1m) is similar to that for the eastern AS. In 2010, the maximum monthly average SWH (~1.44m) was also observed in July at 11km south of the present study area (Fig. 6a). During November 1997-October 1998, the monthly average SWH in July is 1.3 m at 30km south of the present study and is less than that observed in 2015 and 2010, but the monthly mean SWH is same (1.48 m) in June (Fig. 6a). The annual average SWH is same (1m) during 2010 and 2015 at 15m water depth, but is slightly higher (1.08m) in 1997-98 at 12 m water depth (Sanil Kumar et al., 2001). Also, large (0.2 to 42%) inter-annual changes in the monthly average SWH are observed.

Mean wave periods are mainly between 4 and 8s and during the SW monsoon, but the number of waves with 6-8 s period increased. During the non-monsoon period, not much variation is observed in the distribution of wave periods (Fig. 5b). The inter-annual changes in monthly average mean wave period varied from 2 to 28%. Compared to SWH, the  $T_p$  displays a large temporal variability within one month period (Fig. 4c). The occurrence of these short-term shifts in  $T_p$  with negligible variation in SWH is due to the presence of two wave regimes (swells and the wind-sea) and the predominance of one over the other. Seasonality is also observed in  $T_p$ , with SW monsoon characterized by  $T_p$  of about 8-9s and other seasons by  $T_p$  of about 12-14s (Fig. 5c and Fig. 6d), but the variation in monthly average  $T_p$  is less ( $\sim 3.3$ s) over the annual cycle. The monthly average  $T_p$  is high ( $\sim 13.7$ s) in October and is lowest ( $\sim 10.4$ s) in June. The inter-annual changes in monthly average  $T_p$  varied up to 46% since  $T_p$  is an unstable parameter (Fig. 6d). The measured data indicate that during the SW monsoon, the mean peak swell wavelength is 137 m and the annual mean peak swell wavelength is 140 m.

### 3.2. Spectral wave characteristics

The monthly average wave spectra are computed and plotted to get an insight on wave energy variation with the frequency (Fig. 7a). In all the months, monthly averaged wave spectra are double-peaked. During May to October, both the spectral peaks are in the swell band ( $>8$  s) and in the remaining period, the spectral peaks are in both the swell and wind-sea band. The wave heights are lowest in January followed by February (Fig. 6a). Hence, the monthly average spectral energy density of the wave spectrum is also lowest during January. The spectral energy density increased gradually from January to April with peak frequency around 0.07-0.08 Hz. During June, July, August and September, the double-peaked spectrum is observed with high spectral energy density ( $> 1 \text{ m}^2/\text{Hz}$ ). During June and July, the energy of the high-frequency peak is greater than the low-frequency peak, whereas during August, the first and second peaks have almost same energy, and the energy of the second peak is less than the first during September. The two different peaks observed during these months represent the two different wave systems. The first peak at lower frequency represents long-period swells ( $\sim 14-15$  s), and the second peak corresponds to intermediate-period swells ( $\sim 8-9$  s). Both wave systems have the same propagation direction, i.e., south-southeast (S-SE). In January, April, November and December, the wind-sea peak is at 0.16-0.18 Hz (Fig. 7a).

The short-period waves, waves dominated by local seas (wave period  $< 6$  s) in the measured waves based on the contribution of the surface height variance is only 20-40% and a relatively high percentage is seen during November-April due to the increase in local winds due to the NE monsoon (Fig. 8). The contribution of long-period waves, primarily swells (wave period  $> 12$  s) in the spectral



energy is high (~40%) in March and October. The intermediate-period waves, a mixture of local/regional wind forcing ( $6 \text{ s} \leq \text{wave period} \leq 12 \text{ s}$ ) is high (48 to 61%) from May to September due to the influence of SW monsoon (Fig. 8). The individual waves in each wave record of 30 minutes are also grouped into short-period, intermediate-period and long-period waves based on the wave period (Fig. 9). The number of intermediate-period waves is high (~51.2%) during SW monsoon, while short-period waves are high (~55%) during the remaining period. During SW monsoon, the average height of short-period waves is 0.5 m and that of intermediate-period is 1 m. The presence of long-period waves is 5.6% during the SW monsoon, 8.2% during February-May and 9% during October-January. The swells from the south Indian Ocean and from BoB along with the locally generated wind-seas are responsible for the multi-peaked wave energy spectra.

Figure 10 shows the seasonally averaged directional wave spectra. From the 2D-spectra, mainly 2 different wave systems are clearly visible, one at a lower frequency ( $< 0.1 \text{ Hz}$ ) and another system which is at a higher frequency ( $> 0.1 \text{ Hz}$ ). During the NE monsoon (ONDJ), the spectrum shows double-peaks, with two wave systems, but with decreasing energy. The energy of long-period swells is very low in December and January ( $< 0.4 \text{ m}^2/\text{Hz}/\text{deg}$ ). This is because of the propagation of westward swells generated in the Southern Ocean south of Australia due to the weak austral summer storms and intense austral winter storms (Alves, 2006). Second wave system observed during November-January are short-period waves with period 5-6 s and its direction is between  $131^\circ$  and  $137^\circ$ , i.e., from SE. These short-period waves are due to the domination of wind-seas and young swells produced by the local sea breeze system and NE monsoon respectively. Very high-frequency waves ( $> 0.3 \text{ Hz}$ ) are from  $85$  to  $100^\circ$  in November and from  $120$ - $140^\circ$  in December and January. In February and April, even though spectrum is double-peaked, the energy of the second peak is low, whereas during March the distinct peak at around  $0.3 \text{ Hz}$  is much weak and the spectrum is mainly single-peaked. During May, the spectrum shifts to high energy double peaked system and consist of long-period and intermediate period swells (Fig. 10). In all months very low-frequency ( $\sim 0.035 \text{ Hz}$ ) waves are from  $163$ - $197^\circ$  indicating that the angle between the different wave systems is always less than  $90^\circ$ . The 20-m depth contour of the study area is inclined at  $45^\circ$  and hence most of the waves approach the coast at  $135^\circ$ . On few occasions (e.g., 31 May-1 June, 8-9 September), waves with peak period more than 18 s are observed from  $90$ - $110^\circ$  (Fig. 4c) and the SWH of these waves are around 1 m. In this direction, the land mass is at a distance of  $\sim 1600 \text{ km}$ .

SWH associated with swells ( $f_1 = 0.025$ ,  $f_2=0.12 \text{ Hz}$ ) and wind-seas ( $f_1 = 0.13$ ,  $f_2=0.58 \text{ Hz}$ ) are separated in different direction bands and are presented in Fig. 11. 49% of the sea surface height variance in a year is a result of swells from  $136$  to  $228^\circ$  and 25% are the wind-seas from the same

directional sector. In a year, 12% are wind-seas from 44 to 136° and 7% are the swells from the same directional sector. The waves from 0 to 48° and from 228 to 360° are the waves approaching the buoy location from the coast and in a year these waves contribute ~7% of the sea surface height variance. The wave from the coast are partly due to land breeze and partly the reflected waves (Anoop et al. 2014). Significant percentage of waves (~26%) from 44 to 136° is during October to February (Fig. 11), whereas only 7% are during February-May and 4% during June-September.

The monthly wind rose plots shows that the study location is exposed to mainly two different wind systems, south-westerly and north-easterly (Fig. 12). Weak north-westerly winds are also observed in some months. During June-September, due to the influence of strong SW monsoon, high-speed winds from SW are observed, whereas wind speed decreases and direction changes to NE, from October to January. During February to May, wind speed gradually increases and direction shifts to SW. Short-period waves dominated by local seas are also high during November-April. At the study location, during most of the time of the year, the wind direction is SW. From the monthly average directional wave spectra, it is seen that the study area is exposed to waves from NE to SW. The second wave system, i.e. the wind-seas are higher during May to August due to the high wind speed. Wind speed gradually decreases during September and hence, the wind-sea energy also decreases.

### **3.3. Wind-sea and swell separation based on inverse wave age**

The dominance of swell over wind-sea is evident in inverse wave age also. The degree of coupling between winds and waves is represented by inverse wave age (ratio of wind speed ( $U$ ) from CFSR (Climate Forecast System Reanalysis) to the speed of waves at spectral peak). When the waves and winds are strongly coupled inverse wave age will return high values ( $>0.83$ ) and when swells are present low values ( $<0.83$ ) are observed (Hanley et al., 2010). The average value of inverse wave age during SW monsoon, NE monsoon and Fair Weather period are 0.50, 0.34 and 0.39 respectively, resulting in a swell-driven wave regime (Hanley et al., 2010). The theoretical curve (Eq. 1) for a fully developed wind-sea (Hasselmann et al., 1976) is shown in Fig. 13 by a dashed line. Since the swells are predominant in the area, the wave data in all seasons are below the theoretical fully developed wind-sea curve except during the NE wind-sea. Due to the short fetch, the NE wind-sea move away from the theoretical curve for fully developed conditions. The 6-8 s waves are mainly in the fully-developed condition (Fig. 13).

### 3.4 High frequency tail of wave spectrum

In the last few decades, several studies are carried out to describe the high-frequency end of the wave spectrum and observed that the exponent in the expression for the frequency tail has different values (Siadatmousavi et al., 2012). For growing young wind-seas, Liu (1989) suggested  $f^{-4}$  and  $f^{-3}$  (where  $f$  is the frequency) for fully developed wave spectra. Badulin et al. (2007) recommended  $f^{-4}$  for frequencies dominant of nonlinear interactions. The present study shows that the monthly average wave spectrum for frequencies more than 0.25 Hz has a high-frequency tail of between  $f^{-3.5}$  and  $f^{-2}$  in different months (Fig. 14) and these values confirm that shallow water effects are important in the study area. The spectral tail in the Pierson-Moskowitz and JONSWAP spectra, in deep water, is  $f^{-5}$ . In shallow water, the spectral tail leads to another shape as the dispersion relationship is different. Kitaigorodskii (1975) suggested  $f^{-3}$  tail for shallow water (WMO, 1998). So the change in the high-frequency tail is due to shallow water effects i.e., due to the coastal processes. During the SW monsoon, the high-frequency tail follows  $f^{-3.5}$  from 0.25 to 0.35Hz and is  $f^{-3}$  for frequencies  $> 0.35$  Hz. During the remaining period, high-frequency tail follows  $f^{-3}$  from 0.25 to 0.35Hz and is between  $f^{-2}$  and  $f^{-3}$  for frequencies more than 0.35 Hz (Fig. 14). The specific exponent for the high-frequency tail based on best fit for different months are presented in Figure 14 and the value for the annual fit is close to -2.7, which is not far for -3. This low value is probably due to the strong shallow water depth effect. So the observed deviation from the recommended value (-3) is relatively weak. Amrutha et al. (2016) observed that for frequencies from 0.229 to 0.58Hz at 15 m water depth in eastern AS during January-May, the high-frequency tail has  $f^{-2.5}$  and at 5 m water depth, frequencies from 0.315 to 0.55 Hz has the high-frequency tail  $f^{-3}$ . The study shows that the values observed in the present study are similar to the ones observed in the eastern AS. Also, it is to be noted that the buoys used for wave measurement are not very sensitive to high-frequency waves, and is not very dedicated to measure high-frequency tails of wave spectra. When the measuring system is less sensitive (or precise) in the high-frequency range, the experimental noise level enhances the tail, thus giving lower slope.

### 3.5. Long-term trend in wave height

Many studies indicate inter-annual variations in SWH in the eastern shelf seas of India (Young et al., 2011; Aarnes et al., 2015). While the present study did not show a significant inter-annual variability in annual mean SWH, illustrated by standard deviations of the order of 0.03 m. Aarnes et al. (2015) observed that during 1979-1991, there is an increase (0-5% of annual mean value per decade) of SWH in NIO and from 1992 to 2012, there is a decrease (0-5% of annual mean value per decade). Sanil Kumar and Anoop (2015) reported a weak decreasing trend (maximum ~

1.8 cm/decade) in SWH in the western BoB except along the southern region during 1979-2012. Based on the altimeter data, Kumar et al. (2013) observed that the variation in SWH is almost negligible for a period of 18 years in the NIO. The present study shows a weak decreasing trend ( $\sim 0.5$  cm/decade) in SWH during 1979-2015 based on linear regression using the ERA-Interim reanalysis data (Fig. 15a). Similarly, a weak decreasing trend ( $\sim 1.5$  m/s/decade) is observed in the meridional component of wind compared to the trend of zonal component of wind ( $\sim 8.6$  m/s/decade) (Fig. 15b, c). A larger decreasing trend ( $\sim 11.5$  m/s/decade) is observed in wind speed (Fig. 15d). Student's t-test is performed on the data and the p-value obtained are less than 0.05 for all the parameters. It should be clear that climate trends identified in reanalysis datasets can be greatly influenced by temporal changes in the quality and quantity of the data assimilated into the model (Godoi et al., 2017).

## **4. Discussion**

### **4.1 Role of the shallow water processes on waves in the measurement location**

The relative water depth ( $d/L$ ) based on mean wave period shows that the wave regime is in intermediate and shallow water during 92.1% of the time during the one-year period. The wave characteristics reported here are influenced by bathymetry since the measured data is from intermediate and shallow water. The measured waves also will be influenced by the tidal currents since the tidal range in the study area is 1.43 m during the spring tide and 0.54 m during the neap tide (Indian Tide Tables, 2017) and can generate tidal currents up to 0.3 m/s (Misra et al., 2013). The Indian shore in the study location is relatively straight (Fig. 2). All waves with wavelength greater than 30 m would feel the bottom, and consequently they would be refracted by the sea bottom. The order of magnitude of measured wavelengths is 100-220m, which is much longer than 30m. Any wave coming from offshore (whatever its initial direction) will be refracted, and its propagation direction will be turned towards the shore direction, perpendicular to shoreline). Wave direction in the inner shelf is strongly influenced by the very local bathymetry. Similarly, a shallow water depth will also influence the water wave height (SWH) (shoaling or dissipating depending on the location in the inner region). Wave heights at 15m water depth have different characteristics than wave heights at 100m or more higher depths. Hence, the buoy measured wave data has undergone the shallow water process of refraction, shoaling, bottom friction and resulted in lower SWH compared to that at deep water and also due to these process, there is a large difference in the wave direction between the ERA-Interim and measured data (Table 1).

At the buoy location, the water depth is small relative to the wavelength, and long waves have been refracted by the bottom. Most of the time the wave directionality is confined to a narrow distribution mainly from SSE due to the wave refraction. The open sea swell, outside the inner layer, is probably from S, may be from SW if we look at the wind direction (monsoon is from SW). But in the inner region, clearly Figure 10 show that all the year long, swell is incoming from SSE direction at the buoy location. Wind-seas are less sensitive to the bottom, so their directions show large range. Figure 5d also shows clearly that the main incoming swell direction is  $165^\circ$ , i.e., SSE, and also often  $135^\circ$  which is SE. This proves that the offshore open sea SW swell is refracted in the inner region, turning left with a final SSE incoming direction at the buoy location. During the NE monsoon, the influence of local wind is higher due to the NE winds resulting in larger short-period waves compared to other months. The direction of these waves in the NE monsoon in deep waters will be NE due to the strong wind from that direction (Fig. 12). Since the 30-m depth contour is aligned  $\sim 43^\circ$ , the waves will have direction  $\sim 133^\circ$  (SE) at the measured location due to the wave refraction.

## **4.2 Mechanisms driving the wave height variability**

### **4.2.1 Sea breeze/land breeze**

The sea and land breeze combination is a feature observed in the coastal areas of the subtropics and tropics (Miller et al., 2003). After the withdrawal of Indian summer monsoon and until the onset of next monsoon, especially during November to May, winds in the coastal regions of India are dominated by sea and land breeze. Hence during February, the second peak of the monthly average spectrum is at 0.22 Hz, and they are wind-sea due to the sea breeze (Fig. 7a). It can be seen that, during April, the peak direction of second wave system is  $174^\circ$ , which indicates waves are approaching from the south. Earlier study (Simpson et al., 2007) during the SW monsoon period on the variation of sea breeze over the east coast of India showed that the wind direction during the early morning hours are westerly (land breeze) and at around 0230 UTC (0800 IST), the wind direction changes to southeasterly due to the sea breeze. Hence, the second wave system at 0.18 Hz, observed here is generated due to the sea breeze system. Many researchers studied the diurnal variation in wave parameters due to the sea breeze in the eastern AS (e.g., Glejin et al., 2013). During November–January, the short-period waves observed are due to the domination of wind-seas and young swells produced by the local sea breeze and NE monsoon (Fig. 9). The sea/land breeze influence on the waves is observed mainly during November–April (Fig. 16). During October–December, maximum SWH is observed at 1400 UTC (1930 IST) and the minimum value is at 2300 UTC (0430 IST). During January–April, the maximum SWH is at 1000–1300 UTC (1530–1830 IST). The diurnal variation in SWH during January–April is 0.15 m and is less compared to the variation

(~0.2 m) observed along the west coast of India (Sanil Kumar et al., 2014). During the SW monsoon season, negligible diurnal variation is observed due to the strong monsoon winds.

#### **4.2.2 SW monsoon**

The SW monsoon onset is characterized by rapid changes in the prevailing rainfall intensity and wind direction and generally arrive in the southeast BoB and the Andaman Sea by 20 May (Joseph et al., 2006). Advancing through the BoB, by 10 June it touches the Andhra Pradesh coast. In the SW monsoon season, the enhanced south-westerlies in the Indian Ocean strengthen the generated swells. The high waves (SWH~ 3 to 5.5 m) in the eastern AS during the SW monsoon are as a result of the strong cross-equatorial winds of the Findlater Jet (Findlater, 1969), which produces high waves of 4 to 6 m in the western AS and propagate to the eastern AS (Amrutha and Sanil Kumar, 2017). In the study area, SW monsoon wave heights are larger and elevated above 1.5m during 38.4% of the time. SWH exceeded 2m during 146 hr during the SW monsoon period and SWH less than 0.5m is not present during the SW monsoon period. During May and June, the spectral peak frequency shifted to higher frequencies (~0.11 Hz) and with the intensification of SW monsoon, in July and August, the spectral peak shifted further towards higher frequency (~ 0.12 Hz). The wave heights in the northern BoB during the SW monsoon period is lower compared to the eastern AS since the AS branch of monsoon is more powerful than BoB branch, while during October-December, the wave heights are higher in the northern BoB compared to eastern AS (Fig. 6a). The study shows that swells are present in the study region throughout the year are mainly generated by the trade winds and southern extra-tropical storms. During the SW monsoon these swells are superimposed with the young swells and wind-sea generated by the strong monsoon winds. Over the one year period, maximum energy observed in July ( $1.618 \text{ m}^2/\text{Hz}/\text{deg}$  at 0.12 Hz/deg). High energy waves during the SW monsoon are due to the influence of strong SW monsoon winds and are from 165 to 190°.

#### **4.2.3 Tropical cyclones**

The highest SWH of 2.8m is observed on 21 June 2015 and is due to the depression BOB01 formed in BOB during the SW monsoon on 17 June 2015 about 250km east-southeast of Visakhapatnam (IMD, 2015). This depression moved along with the advancing SW monsoon and made landfall on 21 June 2015 over Odisha between Gopalpur and Puri. Since no major cyclone occurred in 2015, the wave data of 2014 measured at location B during the cyclonic storm Hudhud is examined. This cyclone originated from a low-pressure system that formed under the influence of an upper-air cyclonic circulation in the Andaman sea on 6 October 2014 intensified into a severe

cyclonic storm on 9 October 2014 and made landfall about 30 km west-northwest of Visakhapatnam on October 12, noon local time. The maximum sustained wind speeds were 115 knots (Joint Typhoon Warning Center) corresponding to a weak Category 4 hurricane on the Saffir-Simpson Hurricane Wind Scale. When the cyclone centre is 700 km away from the buoy location (Fig. 17a), the SWH started to increase on 9 October 2014 at 0930 UTC from 0.7 m and reached 7.5 m on 12 October 2014 at 1030 UTC due to the cyclone (Fig. 17c). The average SWH during 7-8 October 2014 is 0.73 m and increased to 4.3 m on 12 October 2014 and reduced to 1 m on 15 October 2014 indicating that the influence of cyclone on the waves is only for 6 days. The increase in  $T_{m02}$  before the arrival of the cyclone indicates that the swells generated by the cyclone reached the location before the cyclone (Fig. 17d). The velocity of forward motion of cyclone is  $\sim 3$  m/s, whereas the group velocity of the waves is  $\sim 4.5$  m/s. The peak wave period reduced from 13-15 s to 9-12 s during the cyclone. During the cyclone, the peak frequency shifted from lower (0.06 to 0.08 Hz) to higher frequencies (0.09 to 0.14 Hz) due to the increase in the local wind. Before and after the cyclone, the peak frequency is around 0.06 to 0.08 Hz (Fig. 17e). The peak wave direction before the arrival of the cyclone is from 160 to 180° and during the cyclone the wave direction changed to 110 to 130° (Fig. 17f). Just before the cyclone reaching the buoy location most of the waves are from 90 to 120 and as the cyclone has crossed the measurement location, the waves are from 150 to 180°. The maximum spectral energy density increased from 1 to 112  $\text{m}^2/\text{Hz}$  due to the cyclone (Fig. 17g). The monthly average SWH in October 2015 is slightly higher ( $\sim 1.10$  m) than that ( $\sim 0.93$  m) in October 2014, whereas there is a significant increase in maximum SWH ( $\sim 7.5$  m) compared to that ( $\sim 1.57$  m) in October 2015. Monthly average mean wave period in October reduced to 6.2 s in 2014 from 7.1 s in 2015 due to the cyclone.

#### **4.2.4 South Indian Ocean/Southern Ocean swells**

The main characteristic of the spectral data is the existence of large energy in the swell frequency. Wind-sea predominance is not observed in the monthly average wave spectrum and in all the months swells dominated. Long-period waves at the study area are dominated by the presence of mature swells propagating from the Southern Ocean, whereas the intermediate-period swells are dominated by young and mature swells propagating from tropical south Indian Ocean generated by strong easterlies. The swells that propagate from remote sources in the Southern Ocean and the South Indian Ocean result in a mean peak swell wavelength of approximately 220 m in this region.

#### 4.2.5 ENSO and IOD

During the NE monsoon period, an inverse relationship is observed between the seasonal anomaly of SWH and ONI indicating that during strong El Niño years the seasonal average wave height is relatively low. Cherchi and Navarra (2013) reported that strong El Niño years are expected to have a weak monsoon. During other seasons, the influence of ENSO on wave height is not significant. Very strong El Niño years ( $ONI \geq 2.0$ ) are 1982-83, 1997-98 and 2015-2016 and moderate ( $ONI \sim 1.0$  to 1.4), years are 1986-87, 1987-88, 1991-92, 2002-2003, 2009-2010. During October-January, the ONI is observed to have a negative correlation with the SWH anomaly in 1982, 2009, 2015 and during February-May in 1998 (Fig. 18). Excluding the strong and moderate El Niño years resulted in a correlation coefficient of 0.62 between SWH anomaly and ONI, whereas the correlation coefficient for all years is 0.79. To check whether correlation is significant, the t-test method is used. The confidence of the correlation calculated between wave height and the ONI is above 85%. The significant confidence levels show that the ENSO has impacts on the variations in wave height. During June-September, the negative seasonal SWH anomaly is higher in 1984, 1987 and 2015. The correlation coefficient between SWH anomaly and ONI for June-September is 0.64 and when 1984, 1987 and 2015 are removed, a low correlation coefficient (0.56) is observed. Since the wind is the major generating force of surface waves in the Ocean, the wind anomaly caused by IOD and ENSO (Schott et al., 2009) induce the change in wave climate. The peak of El Niño events reduce the winds in the equatorial Indian Ocean (Taschetto et al., 2011) and this may be the reason for the reduction in SWH. The IOD induced changes in the equatorial SST and sea level pressure influenced the wave climate of eastern AS in October since the changes in SST are closely associated with changes in surface winds (Yamagata et al., 2004; Anoop et al., 2016). During the peak phase of the positive IOD, equatorial winds reverse direction from westerlies to easterlies (Yamagata et al., 2004). In the study area, during 1982, 1997 and 2015, which are the positive IOD years, an inverse relationship is observed between the NE monsoon seasonal anomaly of SWH and DMI (Fig. 18). The correlation coefficient between SWH anomaly and DMI for all years is 0.33 and it reduces to 0.29 when the years 1982, 1997 and 2015 are removed. In the eastern AS, the reduction in wave height during positive IOD is due to the reduction in wind-seas as observed by Anoop et al. (2016). Some evidence on the weak connection between the wave heights and climate patterns are presented in this paper. Detailed investigation on the causes are beyond the scope of the present work and will be attempted in future work.



## 5. Conclusions

SW monsoon period is characterized by large waves ( $SWH > 1.5$  m) with mean directions spreading from south to south-east and NE monsoon is characterized by smaller waves with east to south-east directions. The occurrence of tropical cyclone generates high waves ( $SWH > 7$  m) for short period (5 to 6 days). The wave characteristics reported here are influenced by bathymetry since the measured data is from intermediate/shallow water. With contributions of energy propagated from distant regions and energy generated locally, the wave spectrum exhibits multiple wave energy peaks. The contribution of long-period waves, primarily swells (wave period  $> 12$  s) is high (~40%) in March and October, whereas the intermediate-period waves ( $6 \text{ s} \leq \text{wave period} \leq 12 \text{ s}$ ), mixture of local/regional wind forcing is high (48 to 61%) from May-September due to the influence of SW monsoon. Due to the short fetch, the NE wind-seas are not in fully developed conditions, whereas the 6-8 s waves are mainly in the fully-developed condition. 49% of the sea surface height variance in a year is a result of swells from  $136$  to  $228^\circ$  and 25% are the wind-seas from the same directional sector. Another interesting feature is that most of the time, the wave directionality is confined to a narrow distribution. The lower values of inverse wave age indicate that the study area is a swell-driven wave regime. The exponent used in the expression for the high-frequency ( $>0.25$  Hz) tail of the wave spectrum deviates from the recommended values and is between -3.5 and -2. There is a large difference in the wave characteristics in the BoB compared to the AS during the same period. In 2015, high waves are observed in the AS during June (monthly average SWH is 2 m), whereas in the BoB, high waves are in July (1.56 m). Large-scale inter-annual atmospheric changes (ENSO and IOD) caused changes in the wave climate of the north-western BoB. During 1979-2015, large (0.2 to 42%) inter-annual changes in the monthly average SWH are observed, but the inter-annual changes in annual mean SWH in the study area are negligible.

## Acknowledgments

We acknowledge the financial support given by the CSIR-NIO to conduct this research. We thank Dr. B.P.Rao, Mr.P.Ganapathi and Mr. M.Sreenu, CSIR-NIO, Regional Centre, Visakhapatnam for their technical help during the deployment and recovery of the waverider buoy. We thank Mr. Jai Singh and Mrs. Kirti Dubhashi, technical assistant at CSIR-NIO, for the help during data analysis. This research would not have been complete without the availability of the ERA-Interim data provided by the ECMWF. The bathymetry used in Figure 1 is reproduced from GEBCO Sheet G.08 compiled by R.L. Fisher of the Scripps Institution of Oceanography and extracted from the GEBCO Digital Atlas published by the British Oceanographic Data Centre on behalf of the IOC and IHO 2003. We thank Earth System Science Organization-INCOIS, Ministry of Earth Sciences,

Government of India for providing the data at Location B. The valuable comments from three anonymous reviewers and the Editor helped us to improve the manuscript considerably. This work forms part of the Ph.D. Thesis of M. Anjali Nair registered at Goa University. This has NIO contribution No. ....

## References

- Aarnes, O.J, Abdalla, S, Bidlot, J. R, Breivik, Ø, 2015. Marine wind and wave height trends at different ERA-Interim forecast ranges. *Journal of Climate*, 28(2), 819-37.
- Alves, J.H, 2006. Numerical modeling of ocean swell contributions to the global wind-wave climate. *Ocean Model*, 11, 98–122.
- Amrutha, M.M, Sanil Kumar, V, 2017. Characteristics of high monsoon wind-waves observed at multiple stations in the eastern Arabian Sea, *Ocean Science Discussions*, <https://doi.org/10.5194/os-2017-84>.
- Amrutha, M.M, Sanil Kumar, V, Singh, J, 2016. Changes in nearshore waves during the active sea/land breeze period off Vengurla, central west coast of India. *Ann. Geophys.* 34, 215-226.
- Amrutha, M.M, Sanil Kumar, V, Anoop, T. R, Balakrishnan Nair, T.M, Nherakkol, A, Jeyakumar, C, 2014. Waves off Gopalpur, northern Bay of Bengal during Cyclone Phailin. *Ann. Geophys.* 32, 1073-1083.
- Anoop, T.R, Sanil Kumar, V, Shanas, P.R, Johnson, G, Amrutha, M.M, 2016. Indian Ocean Dipole modulated wave climate of eastern Arabian Sea. *Ocean Science*, 12(2), 369-378.
- Anoop, T.R, Sanil Kumar, V, Shanas P.R, Johnson, G, 2015. Surface Wave Climatology and Its Variability in the North Indian Ocean Based on ERA-Interim Reanalysis. *J. Atmospheric and Oceanic Technology*, 32(7), 1372-1385.
- Badulin, S.I, Babanin, A.V, Zaharov, V.E, Resio, D, 2007. Weakly turbulent laws of wind wave growth. *J. Fluid Mech*, 591, 339–378.
- Balaguru, K, Taraphdar, S, Leung, L.R, Foltz, G.R, 2014. Increase in the intensity of postmonsoon Bay of Bengal tropical cyclones. *Geophys. Res. Lett.* 41(10), 3594–3601.
- Cherchi, A, Navarra, A, 2013. Influence of ENSO and of the Indian Ocean Dipole on the Indian summer monsoon variability. *Climate dynamics*, 41(1), 81-103.
- Datawell 2009. *Datawell Waverider Reference Manual*. Datawell BV oceanographic instruments. The Netherlands. pp 123.
- Dee, D.P et al, 2011. The ERA-Interim reanalysis: Configuration and performance of the data assimilation system. *Q J R Meteorol. Soc.* 137, 553-597.
- Dodet, G, Bertin, X, Taborda, R, 2010. Wave climate variability in the North-East Atlantic Ocean over the last six decades. *Ocean Modeling* 31(3), 120-31.

- Girishkumar, M.S and Ravichandran, M, 2012. The influences of ENSO on tropical cyclone activity in the Bay of Bengal during October–December. *J. Geophys. Res.* 117, C02033, doi:10.1029/2011JC007417.
- Glejin, J, Sanil Kumar, V, Balakrishnan Nair, T.M, Singh, J, 2013. Influence of winds on temporally varying short and long-period gravity waves in the near shore regions of the eastern Arabian Sea. *Ocean Science*, 9 (2), 343-353.
- Godoi, V.A, Bryan, K.R, Stephens, S.A, Gorman, R.C, 2017. Extreme waves in New Zealand waters, *Ocean Modelling* 117, 97–110.
- Hanley, K.E, Belcher, S.E, Sullivan, P.P, 2010. A global climatology of wind–wave interaction. *J. Phys. Oceanogr.* 40,1263–1282.
- Hanson, J.L, Phillips, O.M, 2001. Automated analysis of ocean surface directional wave spectra. *Journal of atmospheric and oceanic technology*, 18, 277-293.
- Hansen, J., Sato, M. and Ruedy, R., 2012. Perception of climate change. *Proc. National Academy of Sciences*, 109 (37), E2415-E2423.
- Harley, M.D, Turner, I.L, Short, A.D, Ranasinghe, R, 2010. Interannual variability and controls of the Sydney wave climate. *Int. J. Climatol.* 30, 1332–1335.
- Hasselmann, K, Ross, D.B, Miller, P, Sell, W, 1976. A parametric wave prediction model. *J. Phys. Oceanogr.* 6, 200-228.
- Hemer, M.A, Church, J.A. and Hunter, J.R, 2010. Variability and trends in the directional wave climate of the Southern Hemisphere. *International Journal of Climatology*, 30(4), 475-91.
- IMD. 2015. Tropical Weather Outlook - 21/0600z. India Meteorological Department. New Delhi. Accessed on 20 August 2017.
- Indian Tide Tables, 2017. Indian and selected Foreign Ports. Survey of India, Government of India, New Delhi, 238p.
- Izaguirre, C, Méndez, F.J, Menéndez, M., Losada, I.J, 2011. Global extreme wave height variability based on satellite data. *Geophys. Res. Lett.* 1: 38(10). doi:10.1029/2011GL047302.
- Johnson, G, Sanil Kumar, V, Balakrishnan Nair, T.M, 2013. Monsoon and cyclone induced wave climate over the near shore waters off Puduchery, south western Bay of Bengal. *Ocean Eng.* 72, 277–286. doi:10.1016/j.oceaneng.2013.07.013.
- Joseph, P.V, Sooraj, K. P, Rajan, C. K, 2006. The summer monsoon onset process over South Asia and an objective method for the date of monsoon onset over Kerala. *International journal of Climatology* 26.13: 1871-1893.
- Kinsman, B, 1965. Wind waves: their generation and propagation on the ocean surface. Prentice-Hall. 676 pp.
- Kitaigorodskii, S.A, Krasitskii, V.P, Zaslavskii, M.M, 1975. Phillips theory of equilibrium range in spectra of wind-generated gravity-waves. *J. Phys. Oceanogr.* 5 (3), 410–420.

- Kuik, A.J, Van Vledder, G.P, Holthuijsen, L.H, 1988. A method for the routine analysis of pitch-and-roll buoy wave data. *J. Phys. Oceanogr.* 18,1020-34.
- Kumar, D, Sannasiraj, S.A, Sundar, V. and Polnikov, V.G, 2013. Wind-Wave Characteristics and Climate Variability in the Indian Ocean Region Using Altimeter Data. *Marine Geodesy*, 36, 303-313.
- Liu, P.C, 1989. On the slope of the equilibrium range in the frequency-spectrum of wind-waves. *Journal of Geophysical Research, Oceans* 94 (C4), 5017–5023.
- Liu, Q, Babanin, A. V, Zieger, S, Young, I. R, Guan, C, 2016. Wind and Wave Climate in the Arctic Ocean as Observed by Altimeters. *J. Climate* 29 (22), 7957–7975. URL <http://journals.ametsoc.org/doi/10.1175/JCLI-D-16-0219.1>.
- Longuet-Higgins, M.S, Stewart, R.W, 1964. Radiation stresses in water waves; a physical discussion, with applications. In *Deep Sea Research and Oceanographic Abstracts*. Elsevier, Vol. 11, No. 4, pp 529-562.
- Lopez, H, Kirtman, B.P, 2016. Investigating the seasonal predictability of significant wave height in the West Pacific and Indian Oceans. *Geophys. Res. Lett.*, 43: 3451–3458. doi:10.1002/2016GL068653.
- Ludka, B.C, Gallien, T.W, Crosby, S.C, Guza, R.T, 2016. Mid-El Niño erosion at nourished and unnourished Southern California beaches. *Geophys. Res. Lett.*, 43, doi:10.1002/2016GL068612.
- Miller, S.T, Keim, B.D, Talbot, R.W, Mao, H, 2003. Sea breeze: Structure, forecasting, and impacts. *Reviews of geophysics*, 1, 41(3).
- Misra, S.K., Chandramohan, P., Murty, A.S., Panigrahi, J.K., Mahadevan, R., 2013. Nature of the tide induced flow field along the East Coast of India, *International Journal of Oceans and Oceanography* ISSN 0973-2667, 7, 57-71.
- Patra, S.K. et al, 2016. Cyclone and monsoonal wave characteristics of northwestern Bay of Bengal: long-term observations and modeling. *Natural Hazards*, 82, 1051–1073. doi 10.1007/s11069-016-2233-0.
- Philander, S.G, El Nino, La Nina and the Southern Oscillation. *International Geophysical Series*, Academic Press, (46), 293, 1990.
- Portilla-Yandún, J, Cavaleri, L, Van Vledder, G.P, 2015. Wave spectra partitioning and long term statistical distribution. *Ocean Modelling*, 96:148-60.
- Saji, N.H, Goswami, B.N, Vinayachandran, P.N. and Yamagata, T, 1999. A dipole mode in the tropical Indian Ocean. *Nature*, 401(6751), 360-3.
- Sanil Kumar, V, Anoop, T.R, 2015. Spatial and temporal variations of wave height in shelf seas around India. *Natural Hazards*, 78, 1693-706.
- Sanil Kumar, V, George, J, 2016. Influence of Indian summer monsoon variability on the nearshore waves in the eastern Arabian Sea. *Ann. Geophys.* 34, 871–885, 2016. [www.ann-geophys.net/34/871/2016](http://www.ann-geophys.net/34/871/2016).

- Sanil Kumar, V, Dubhashi, K.K, Balakrishnan Nair, T.M, 2014. Spectral wave characteristics off Gangavaram, Bay of Bengal. *J. Oceanography*, 1:70(3):307-21. doi 10.1007/s10872-014-0223-y.
- Sanil Kumar, V, Kumar, K.A., Raju, N.S, 2001. Nearshore processes along Tikkavanipalem beach, Visakhapatnam, India. *J. Coast. Res*, 1, 271-9. doi 10.1007/s10872-014-0223-y.
- Schott, F.A, Xie, S.P, McCreary, J.P, 2009. Indian Ocean circulation and climate variability. *Reviews of Geophysics*, 1:47(1). doi:10.1029/2007RG000245.
- Semedo, A, R. Vettor, O. Breivik, A. Sterl, M. Reistad, C. G. Soares, Lima, D, 2015. The wind-sea and swell waves climate in the Nordic seas. *Ocean Dyn*, 65, 223–240, doi:10.1007/s10236-014-0788-4.
- Semedo, A, Sušelj, K, Rutgersson, A, Sterl, A, 2011. A global view on the wind-sea and swell climate and variability from ERA-40. *Journal of Climate*, 24(5): 1461-1479.
- Shanas, P.R, Sanil Kumar, V, 2015. Trends in surface wind speed and significant wave height as revealed by ERA-Interim wind wave hindcast in the Central Bay of Bengal. *International Journal of Climatology*, 35, 2654-63. doi: 10.1002/joc.4164.
- Siadatmousavi, S.M, Jose, F, Stone, G.W, 2012. On the importance of high frequency tail in third generation wave models. *Coastal Engineering*, 60, 248–260.
- Simpson, M, Warrior, H, Raman, S, Aswathanarayana, P.A, Mohanty, U.C, Suresh, R, 2007. Sea-breeze-initiated rainfall over the east coast of India during the Indian southwest monsoon. *Natural Hazards*, 42(2): 401-13.
- Suresh, R.R, Annapurnaiah, K, Reddy, K.G, Lakshmi, T.N., Nair, T.B, 2010. Wind-sea and swell characteristics off east coast of India during southwest monsoon. *Int. J. Oceans. Oceanogr*, 4:35-44.
- Taschetto, A.S, Sen Gupta, A, Hendon, H.H, Ummenhofer, C.C, England, M.H., 2011. The contribution of Indian Ocean sea surface temperature Anomalies on Australian summer rainfall during El Niño events. *J Clim* 24:3734–3747.
- WMO, 1998. Guide to wave analysis and forecasting, Second edition, World Meteorological Organization (World Meteorological Organization, Geneva, Switzerland, 1998). WMO-No. 702, ISBN 92-63-12702-6.
- Wyrtki, K., 1981. An estimate of equatorial upwelling in the Pacific, *J. Phys. Oceanogr*, 11, 1205–1214, doi:10.1175/1520-0485(1981)011<1205-1214>.doi:10.1175/1520-0485(1981)011,1205-1214.
- Yamagata, T, Behera, S.K, Luo, J.J, Masson, S, Jury, M.R. Rao, S.A, 2004. Coupled ocean-atmosphere variability in the tropical Indian Ocean. *Earth's Climate*, 189-211.
- Young, I.R, Zieger, S., Babanin, A.V, 2011. Global trends in wind speed and wave height. *Science*, 332: 451-5.

Table 1. Comparison statistics for SWH and mean wave period of ERA-Interim data with the measured data during 1 March 2015 to 28 February 2016.

Data period	parameter	r	RMSE	bias	si
Annual	SWH (m)	0.90	0.24	0.14	0.19
February-May		0.93	0.18	0.12	0.15
June-September		0.73	0.30	0.16	0.18
October-January		0.85	0.22	0.15	0.20
Annual	T <sub>m01</sub> (s)	0.72	1.25	0.74	0.14
February-May		0.67	1.38	0.88	0.15
June-September		0.55	0.99	0.55	0.11
October-January		0.81	1.34	0.78	0.16

## Figure Captions

**Figure 1.** Location of wave measurement (pink dot). The colour contour indicates the depth/elevation. The data is based on GEBCO 30 arc-second interval

**Figure 2.** Nearshore bathymetry at Visakhapatnam along with buoy locations. Locations A, B and C indicate the waverider buoy moored site

**Figure 3.** The seasonal average wind pattern in BoB during (a) February-May, (b) June-September and (c) October-January in the year 2015 based on ERA-Interim reanalysis data

**Figure 4.** Time series plot of measured values and the ERA-Interim data; a) significant wave height, b) mean wave period, c) peak wave period and d) mean wave direction

**Figure 5.** Histogram showing the percentage occurrence of a) significant wave heights in bins of 0.5 m, b) mean wave period in bins of 2 s, c) peak wave period in bins of 2 s and d) mean wave direction in bins of 15 deg in different seasons

**Figure 6.** Wave parameters of the monthly average wave spectrum during March 2015 to February 2016. a) significant wave height, b) maximum spectral energy density, c) mean wave period, d) peak wave period, e) mean wave direction. Black thick lines indicates the values at Visakhapatnam and blue dotted line is for Honnavar, location in eastern Arabian Sea at 10 m water depth. Gangavaram data during 2010 (Sanil Kumar et al., 2014) is presented in red line. Tikkavanipalem data during November 1997- October 1998 (Sanil Kumar et al 2001) is also shown

**Figure 7.** Monthly average wave spectrum (top panel) and mean wave direction (bottom panel) during March 2015 to February 2016

**Figure 8.** Monthly average value of contribution of long-period waves ( $T_p > 12$  s), intermediate ( $6 < T_p < 12$  s) and short-period waves ( $T_p < 6$  s)

**Figure 9.** Percentage of short-period ( $T < 6$  s), intermediate-period ( $6 \leq T \leq 12$  s) and long-period ( $T \geq 12$  s) waves measured in each wave record of 30 minutes during 1 March 2015 to 28 February 2016

**Figure 10.** Seasonal and annual average directional wave spectrum. The color bar is for spectral energy density ( $m^2 / Deg/Hz$ ) . The spectral energy is shown in logarithmic scale (base 10). The concentric circles are the frequency in Hz

**Figure 11.** a,d) Percentage of surface height variance from different direction bands (0-44° & 228-360°, 44-136° and 136-228°), b,e) corresponding significant wave height and c,f) the mean wave period. Left panel shows the swells and right panel is for wind-seas

**Figure 12.** Monthly wind rose diagram during March 2015 to February 2016. NCEP CFSR wind data at <http://rda.ucar.edu/pub/cfsr.html> developed by the National Oceanic and Atmospheric Administration (NOAA) is used

**Figure 13.** Plot of  $\log(U/gT_p)$  versus  $\log(U^2/g \text{ SWH})$  stratified by seasons (top panel), peak wave direction (NE and SE) for wind-sea and swell for all the measured data. Dashed line represents the theoretical relation given by Eq. 1.

**Figure 14.** High frequency tail of the wave energy spectra in different months. Frequency tails  $f^{-3.5}$ ,  $f^{-3}$  and  $f^{-2}$  are also shown along with the best fit values

**Figure 15.** Time series plot of annual averaged a) significant wave height, b) energy wave period, c) zonal wind, d) meridional wind and e) wind speed during 1979 to 2015

**Figure 16.** Plot of hourly averaged significant wave height and mean wave period in different months

**Figure 17.** Plot of (a) distance of cyclone centre from the buoy location, (b) wind speed along the cyclone track, (c) time series plot of significant wave height, (d) mean wave period and (e) peak frequency during 6 to 15 October 2014, (f) mean wave direction and (g) spectral energy density with frequency

**Figure 18.** Time series of the seasonal anomaly significant wave height with the Ocean Niño Index and Dipole Mode Index



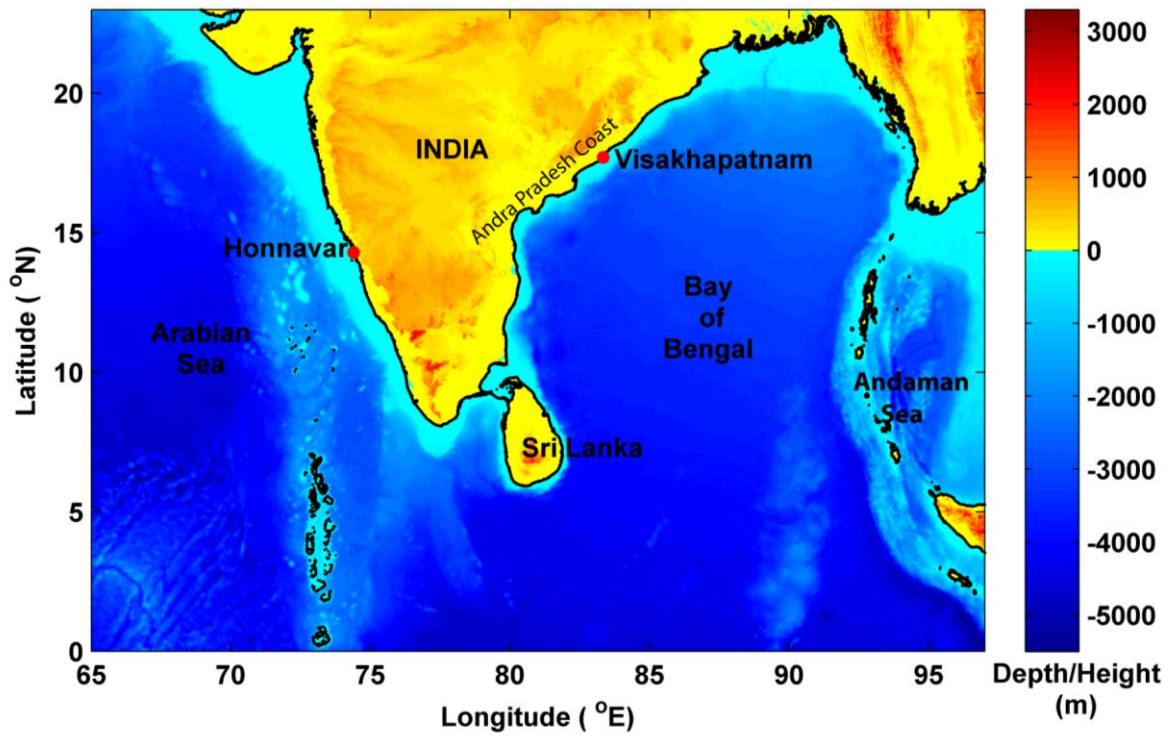


**Figure 1.** Location of wave measurements at Visakhapatnam and Honnavar. The colour contour indicates the depth/elevation. The data is based on GEBCO 30 arc seconds

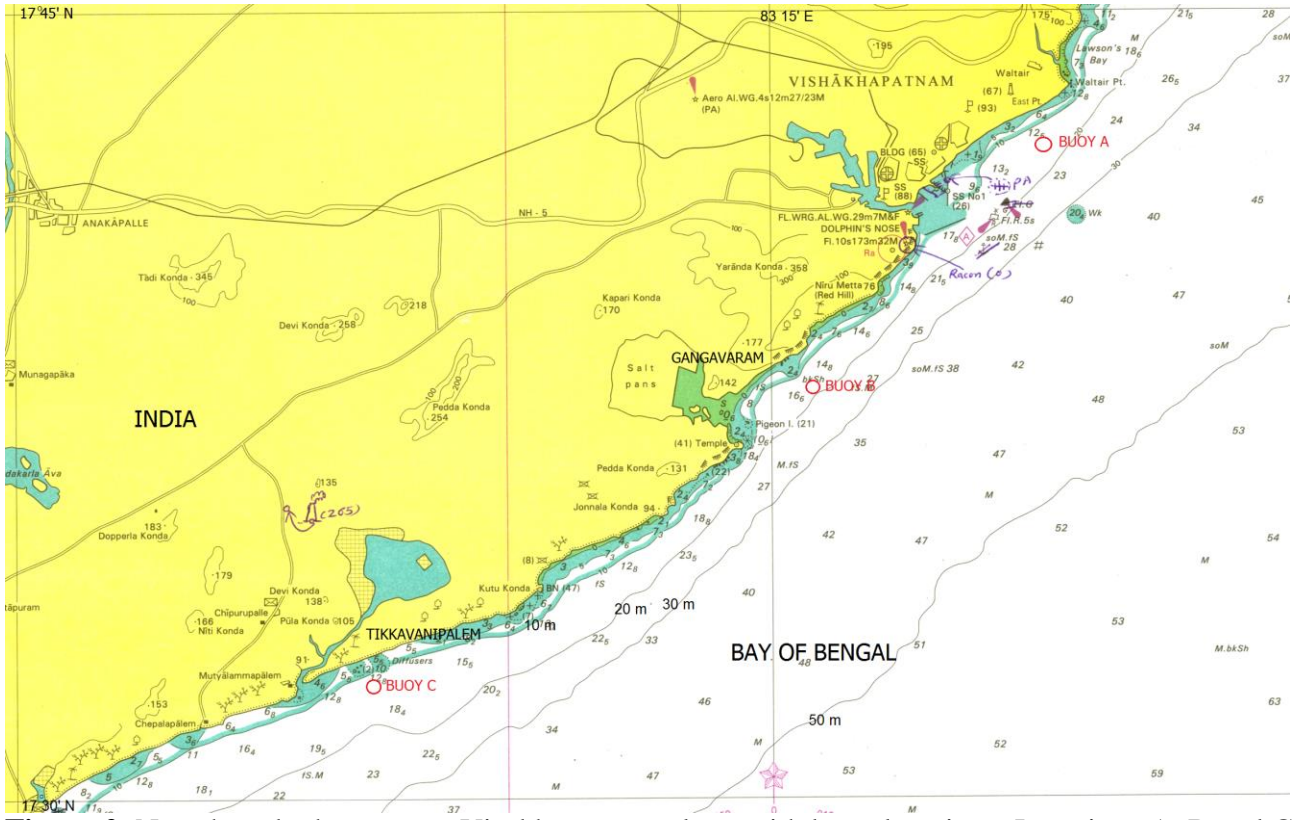


**Figure 2.** Nearshore bathymetry at Visakhapatnam along with buoy locations. Locations A, B and C indicate the waverider buoy moored site.

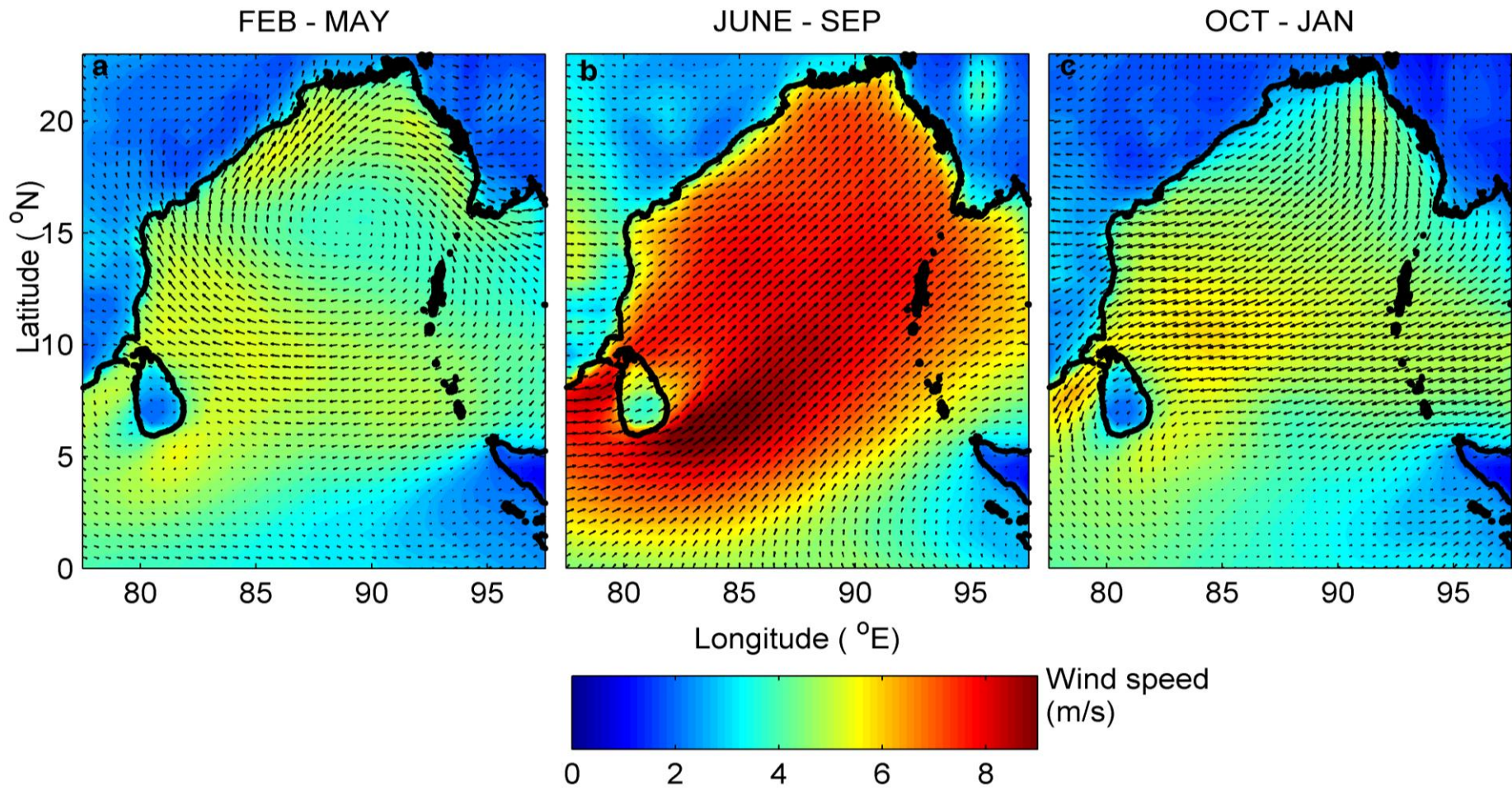


**Figure 3.** The seasonal average wind pattern in BoB during (a) February-May, (b) June-September and (c) October-January in the year 2015 based on ERA-Interim reanalysis data

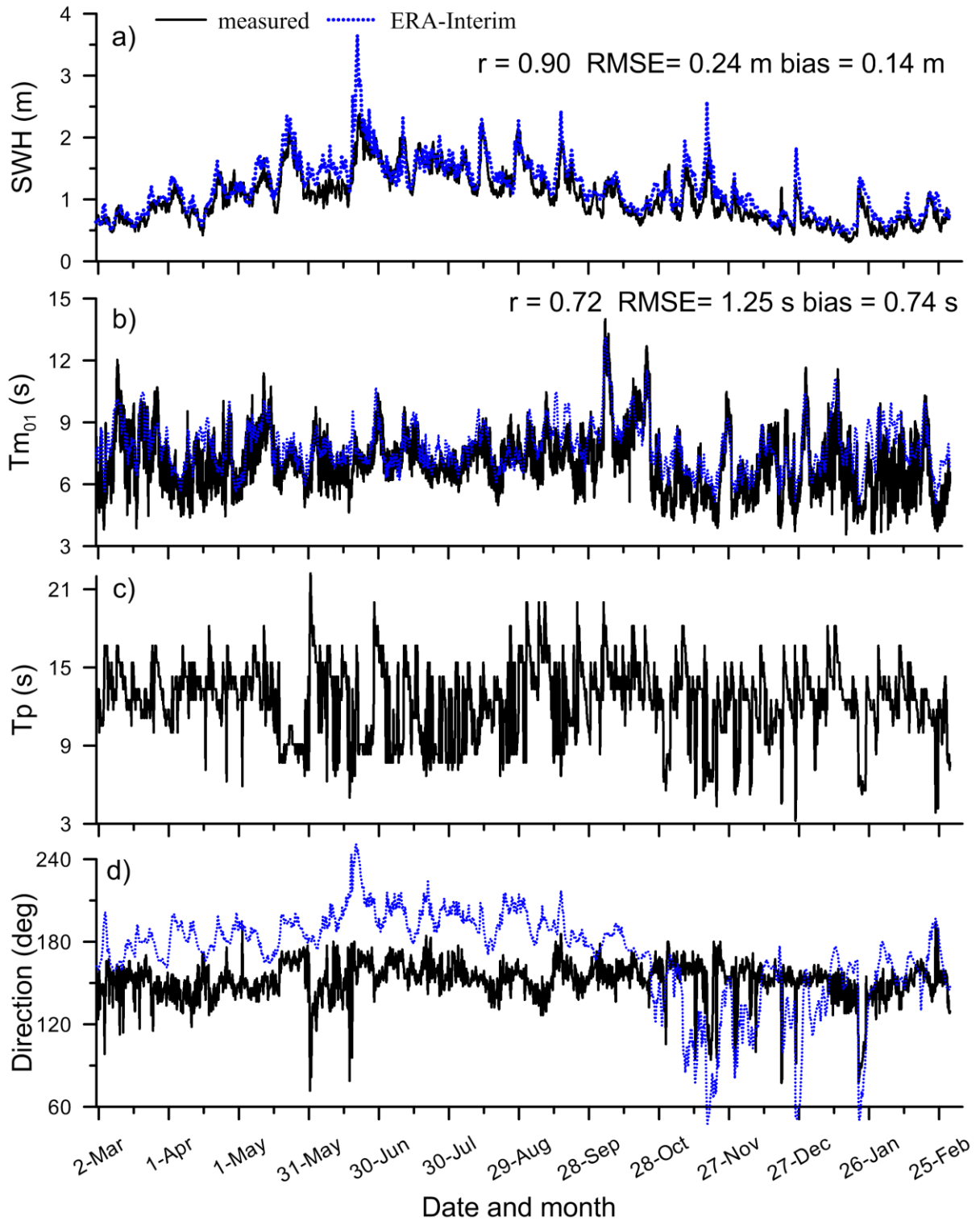


**Figure 4.** Time series plot of measured values and the ERA-Interim data; a) significant wave height, b) mean wave period, c) peak wave period and d) mean wave direction

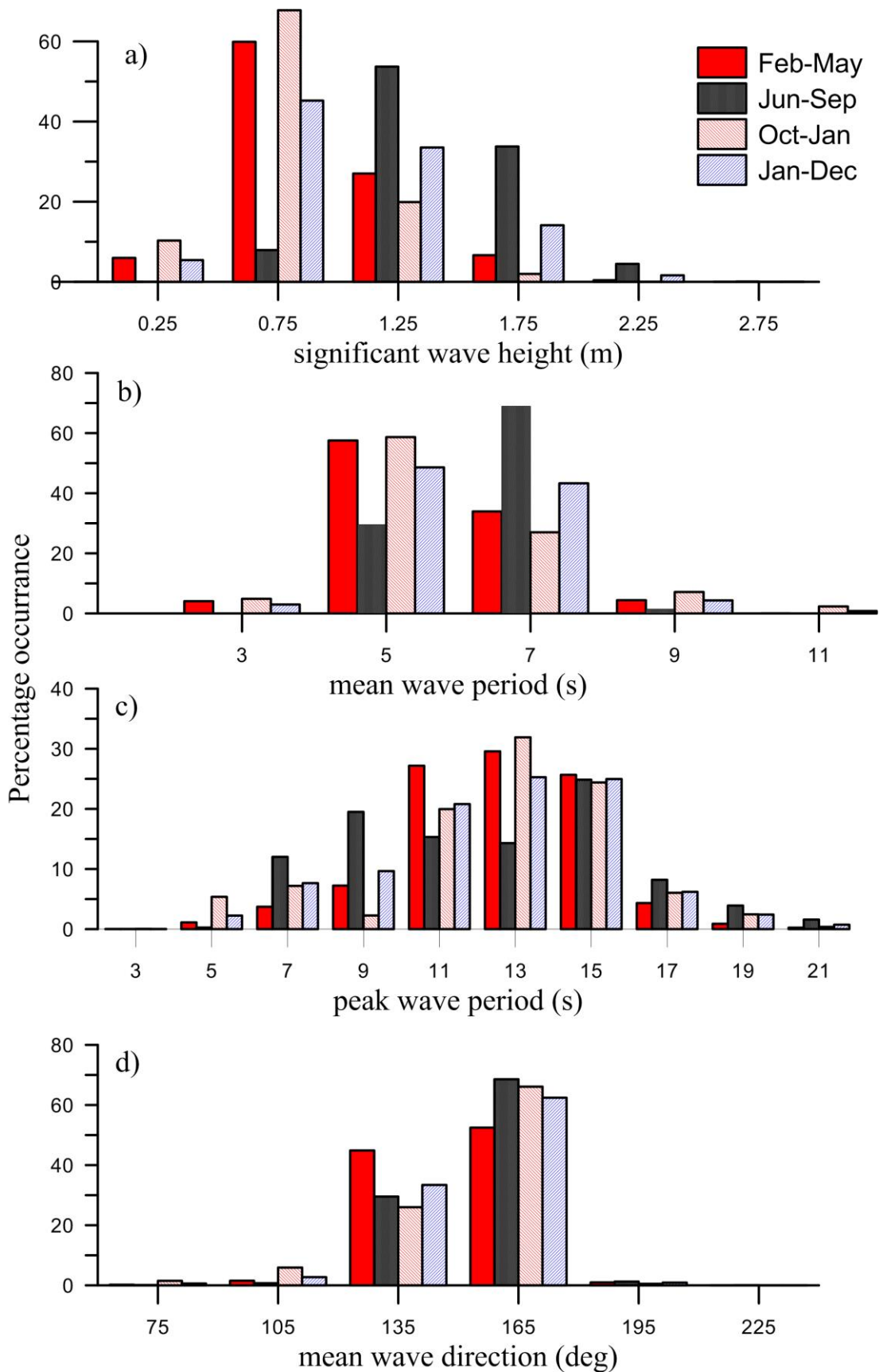


**Figure 5.** Histogram showing the percentage occurrence of a) significant wave heights in bins of 0.5 m, b) mean wave period in bins of 2 s, c) peak wave period in bins of 2 s and d) mean wave direction in bins of 15 deg in different seasons

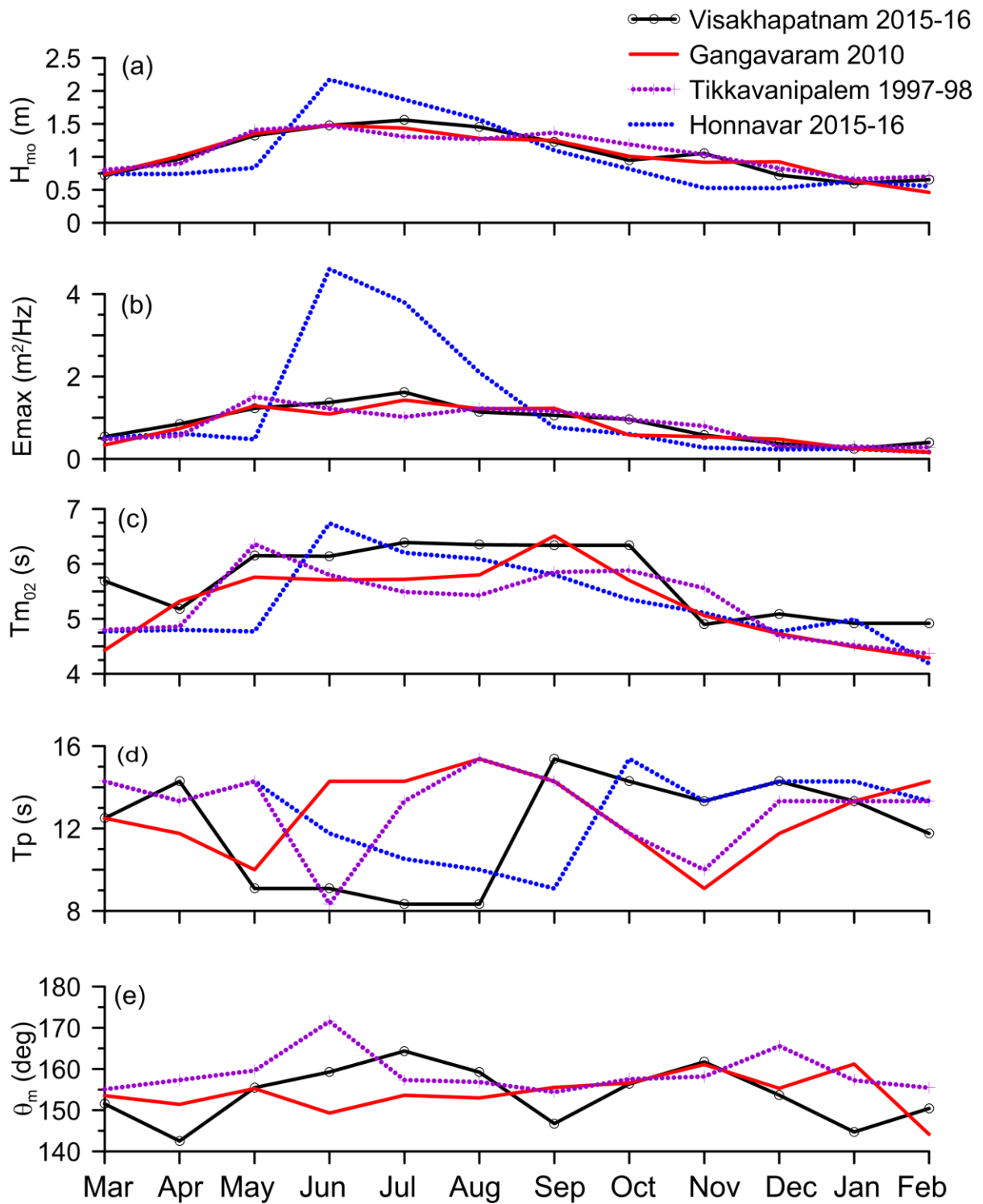


**Figure 6. Wave parameters of the monthly average wave spectrum during March 2015 to February 2016.** a) significant wave height, b) maximum spectral energy density, c) mean wave period, d) peak wave period, e) mean wave direction. Black thick lines indicates the values at Visakhapatnam and blue dotted line is for Honnavar, location in eastern Arabian Sea at 10 m water depth. Gangavaram data during 2010 (Sanil Kumar et al., 2014) is presented in red line. Tikkavanipalem data during November 1997- October 1998 (Sanil Kumar et al., 2001) is also shown

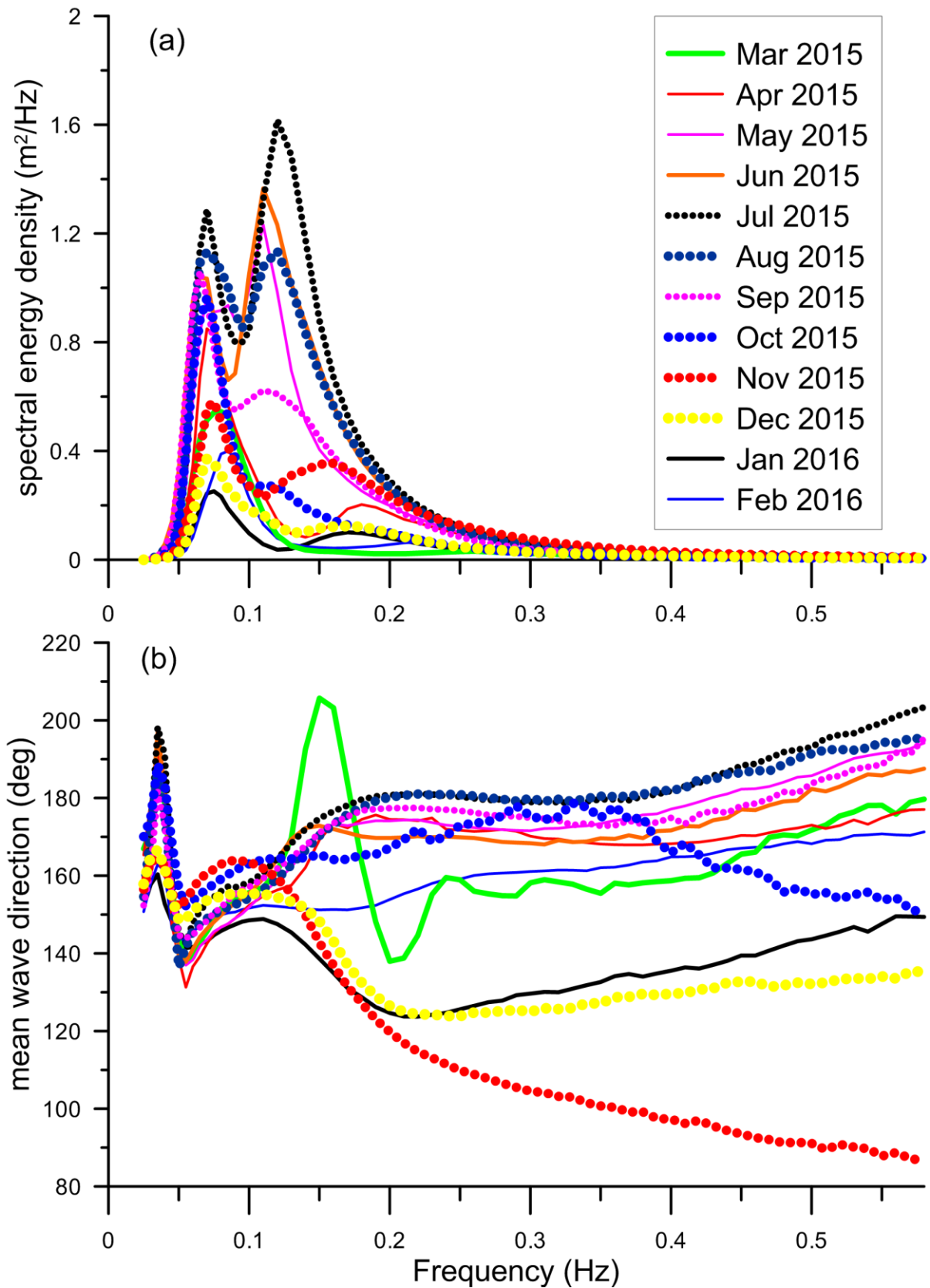


**Figure 7.** Monthly average wave spectrum (top panel) and mean wave direction (bottom panel) during March 2015 to February 2016

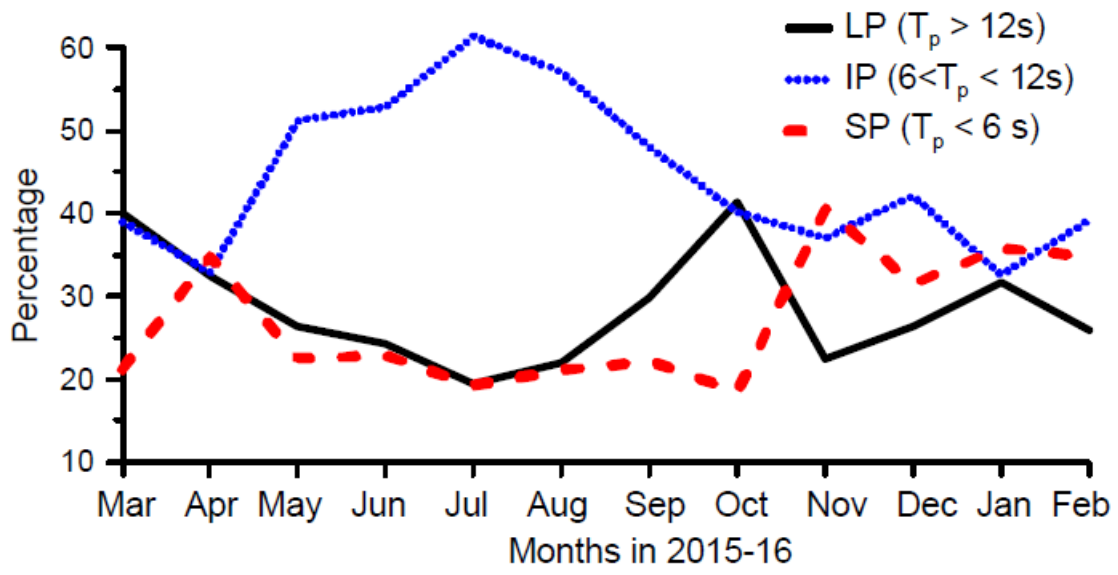
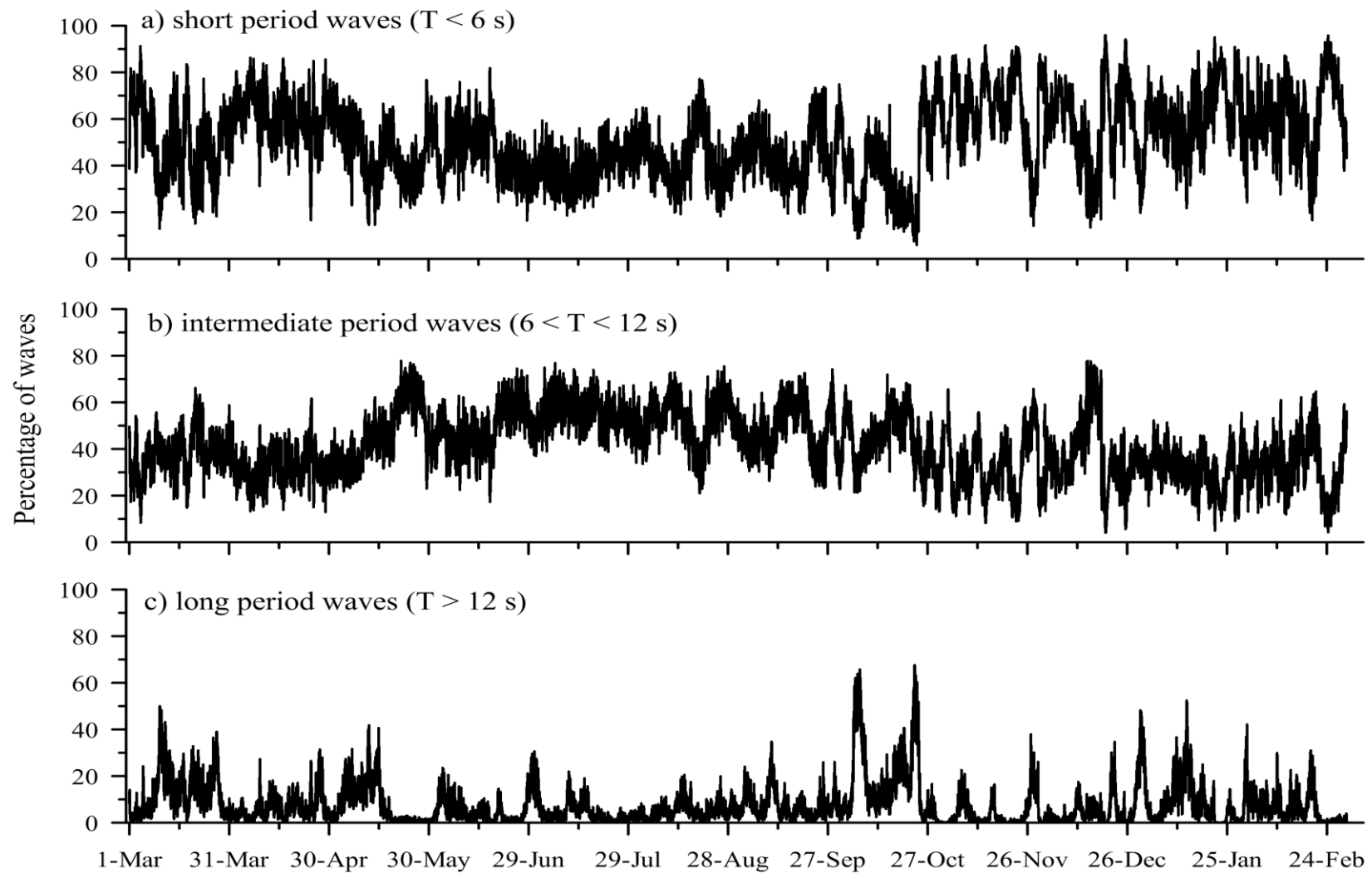


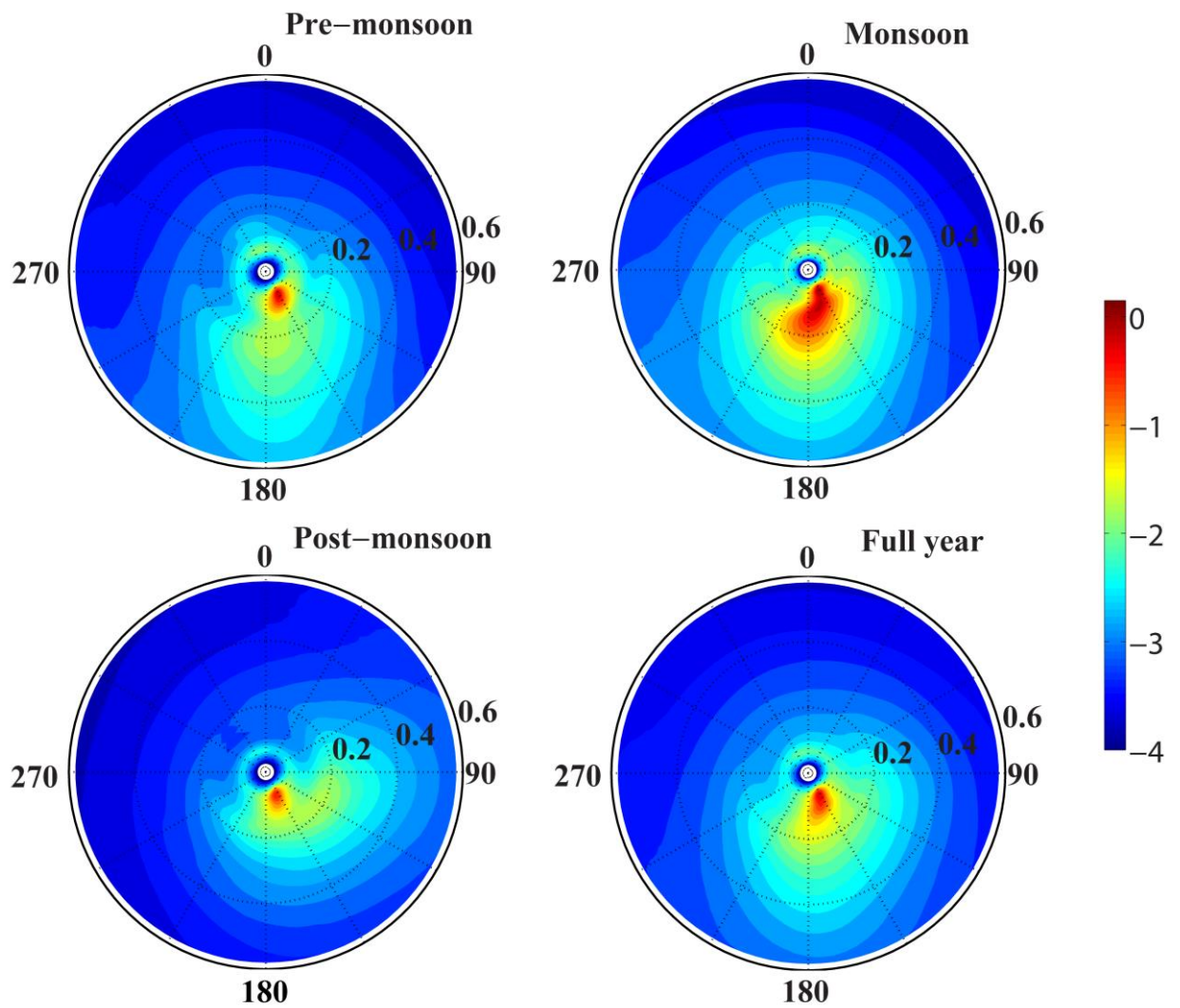
**Figure 8.** Monthly average value of contribution of long-period waves ( $T_p > 12s$ ), intermediate ( $6 < T_p < 12s$ ) and short-period waves ( $T_p < 6s$ )





1 March 2015 to 28 February 2016

**Figure 9.** Percentage of short-period ( $T < 6$  s), intermediate-period ( $6 \leq T \leq 12$  s) and long-period ( $T \geq 12$  s) waves measured in each wave record of 30 minutes during 1 March 2015 to 28 February 2016



**Direction (degrees)/Frequency (Hz)**

**Figure 10.** Seasonal and annual average directional wave spectrum. The color bar is for spectral energy density ( $\text{m}^2/\text{Deg/Hz}$ ). The spectral energy is shown in logarithmic scale (base 10). The concentric circles are the frequency in Hz.



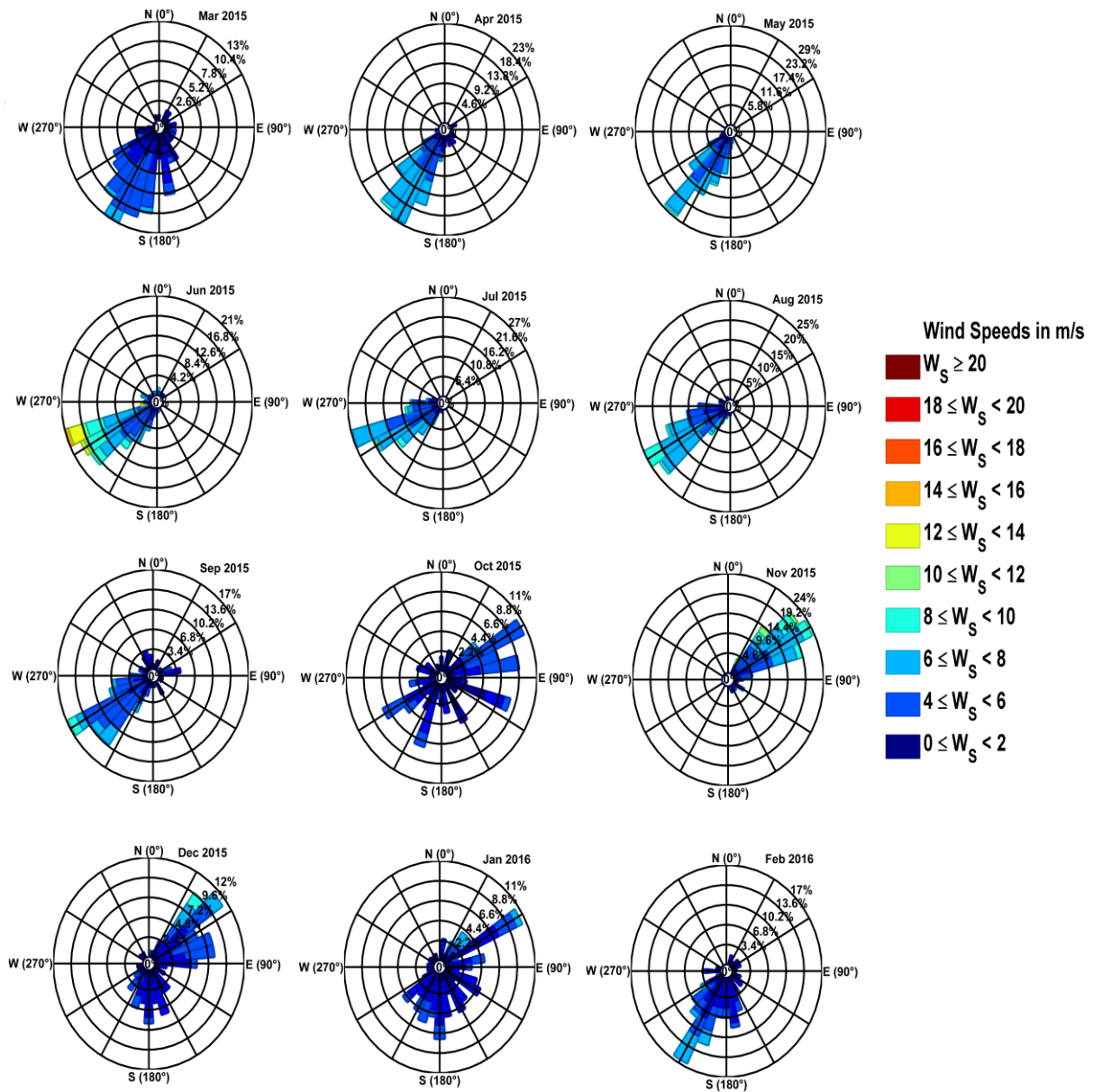
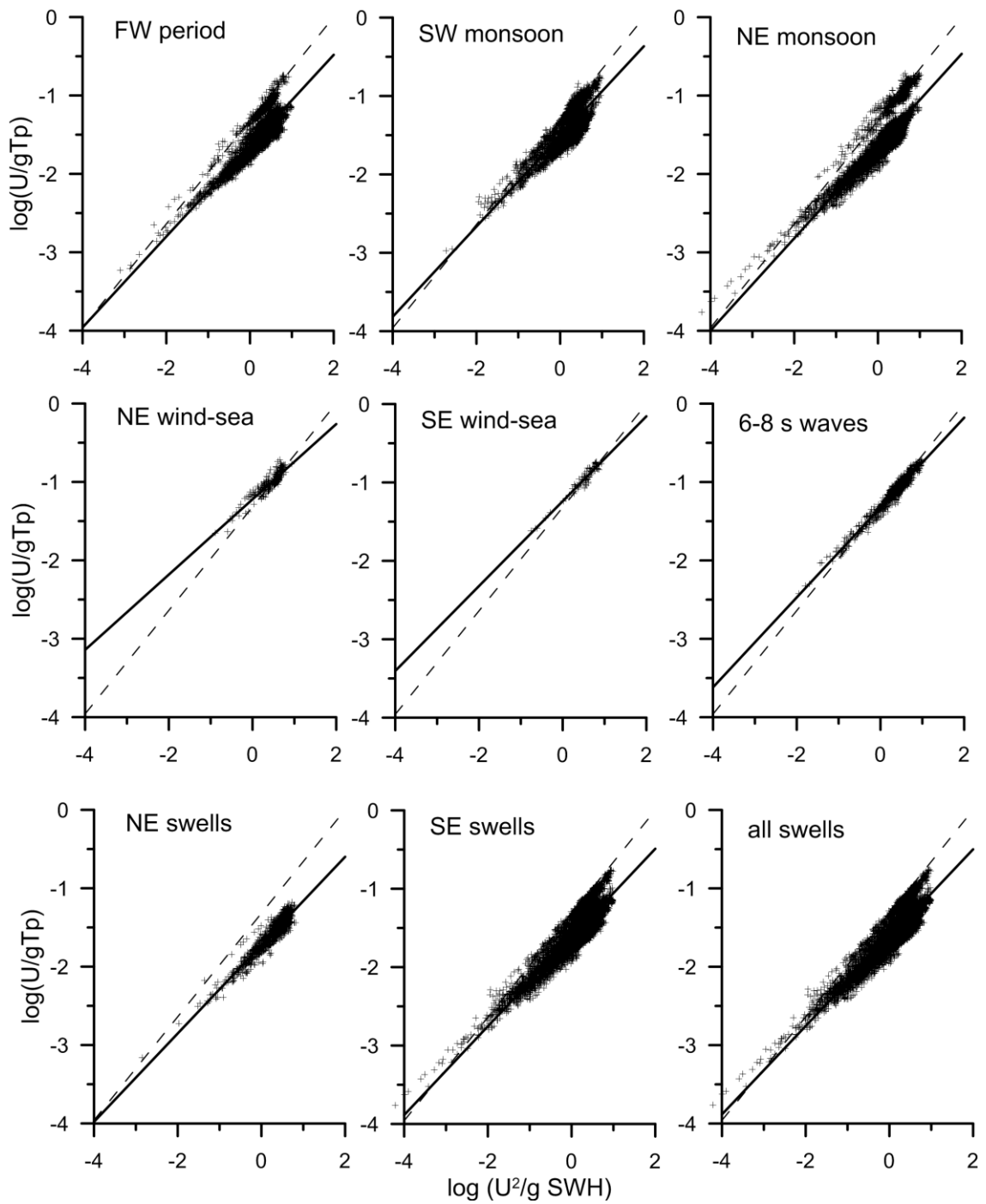
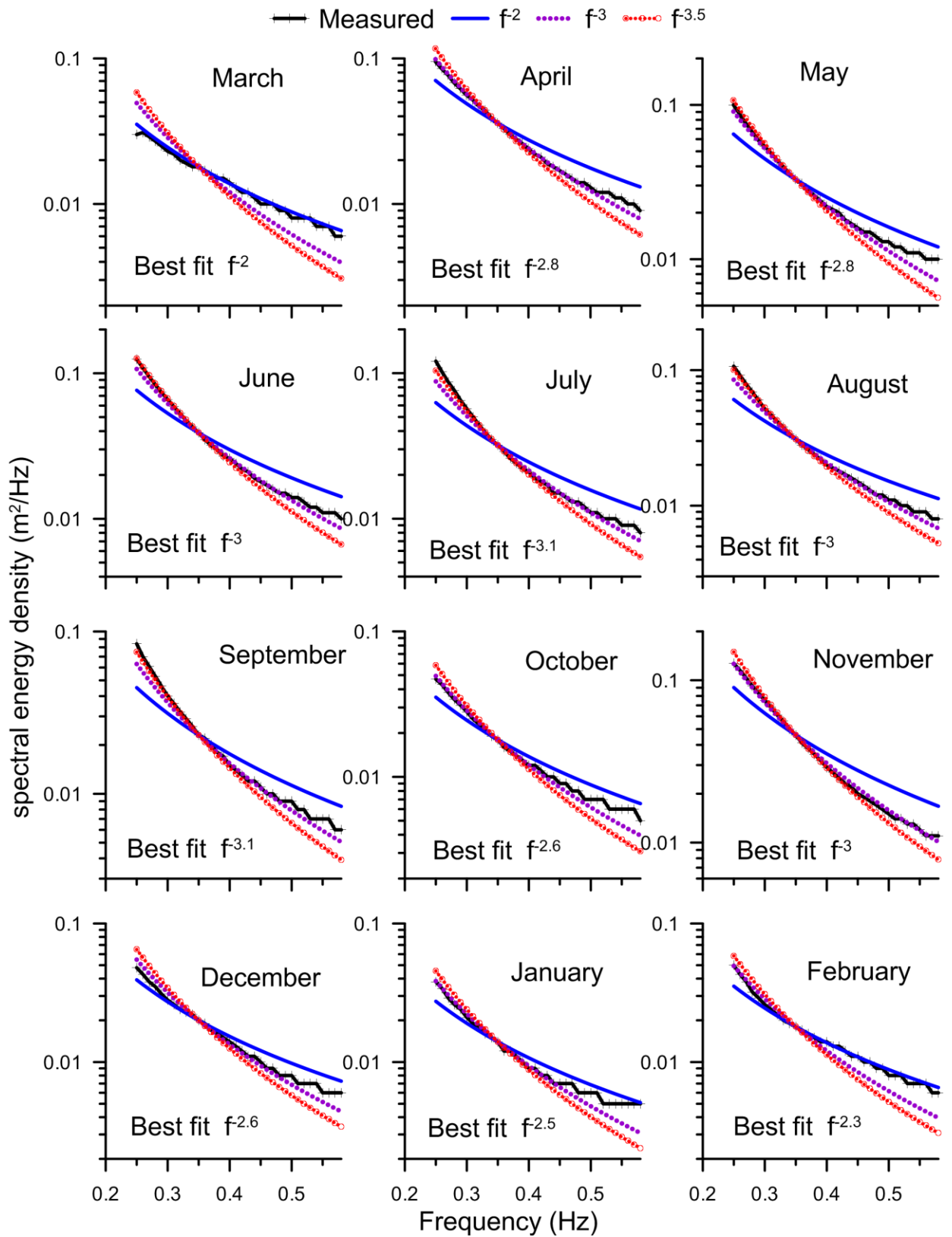


Figure 12. Monthly wind rose diagram during March 2015 to February 2016 based on ECMWF ERA-Interim wind data



**Figure 13.** Plot of  $\log(U/gT_p)$  versus  $\log(U^2/g \text{ SWH})$  stratified by seasons (top panel), peak wave direction (NE and SE) for wind-sea and swell for all the measured data. Dashed line represents the theoretical relation given by Eq. 1



**Figure 14.** High frequency tail of the wave energy spectra in different months. Frequency tails  $f^{3.5}$ ,  $f^3$  and  $f^2$  are also shown along with the best fit values

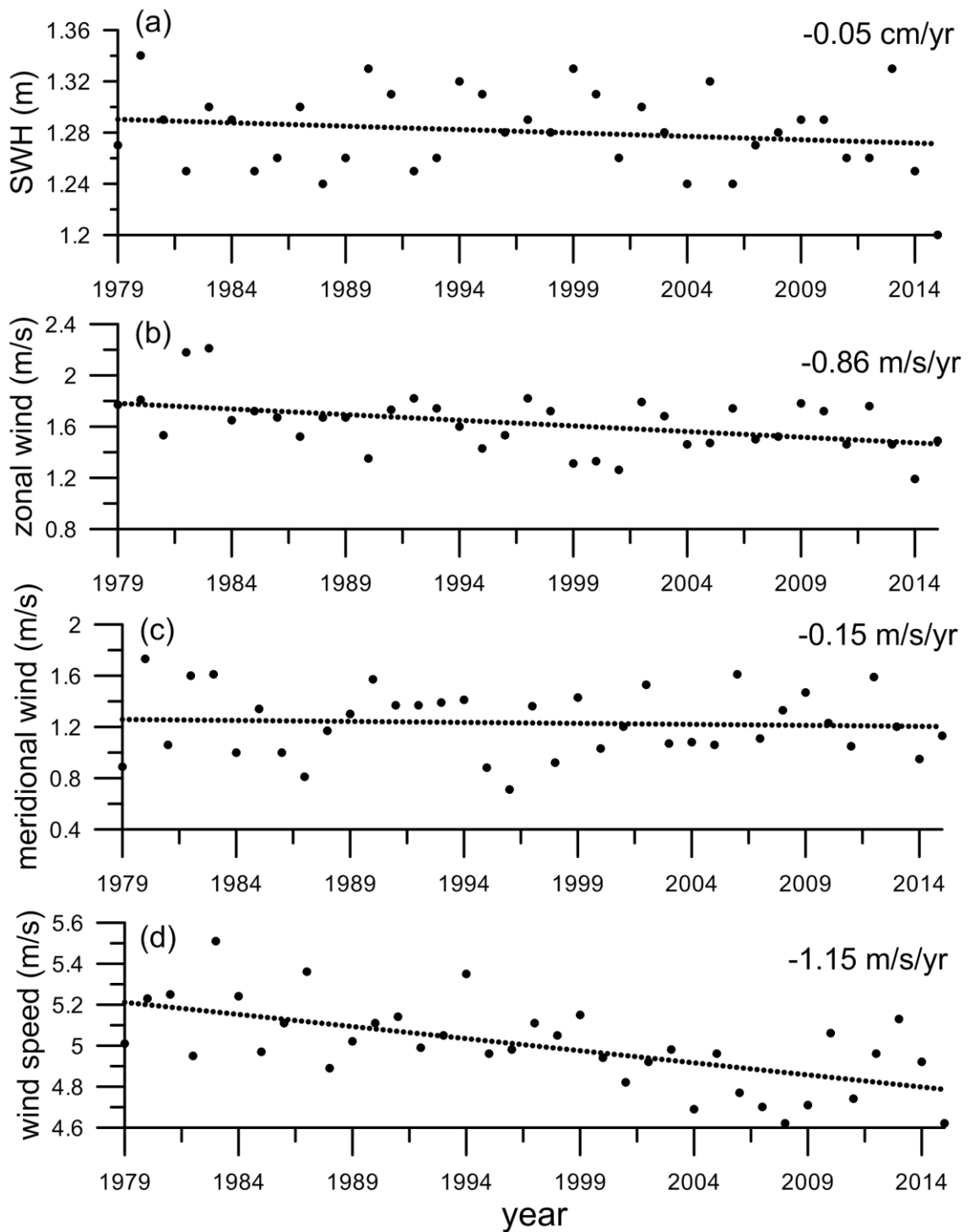


**Figure 15.** Time series plot of annual averaged a) significant wave height, b) zonal component of wind, c) meridional component of wind and d) wind speed during 1979 to 2015

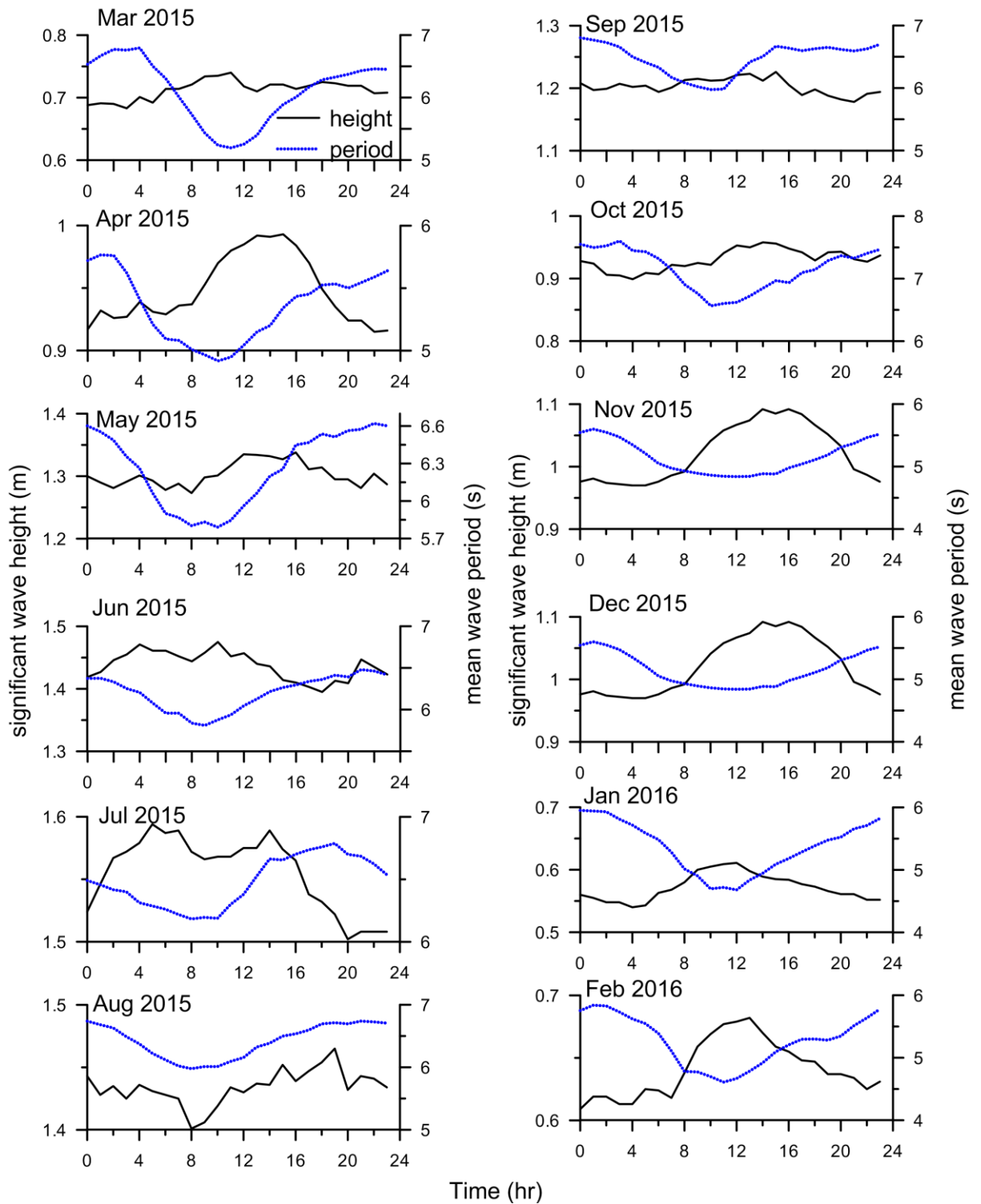


**Figure 16.** Plot of hourly averaged significant wave height and mean wave period in different months



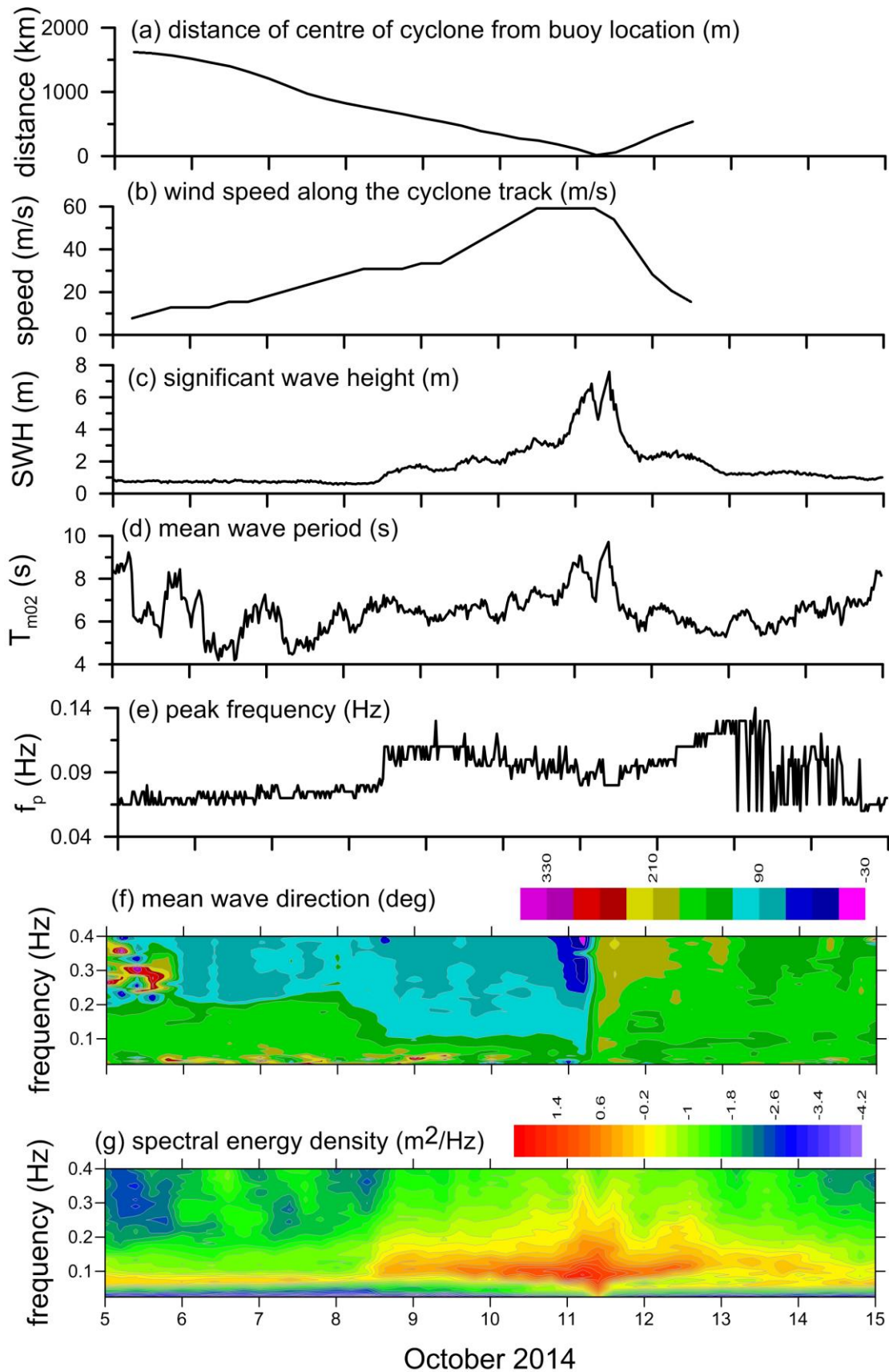


**Figure 17.** Plot of (a) distance of cyclone centre from the buoy location, (b) wind speed along the cyclone track, (c) time series plot of significant wave height, (d) mean wave period and (e) peak frequency during 6 to 15 October 2014, (f) mean wave direction and (g) spectral energy density with frequency

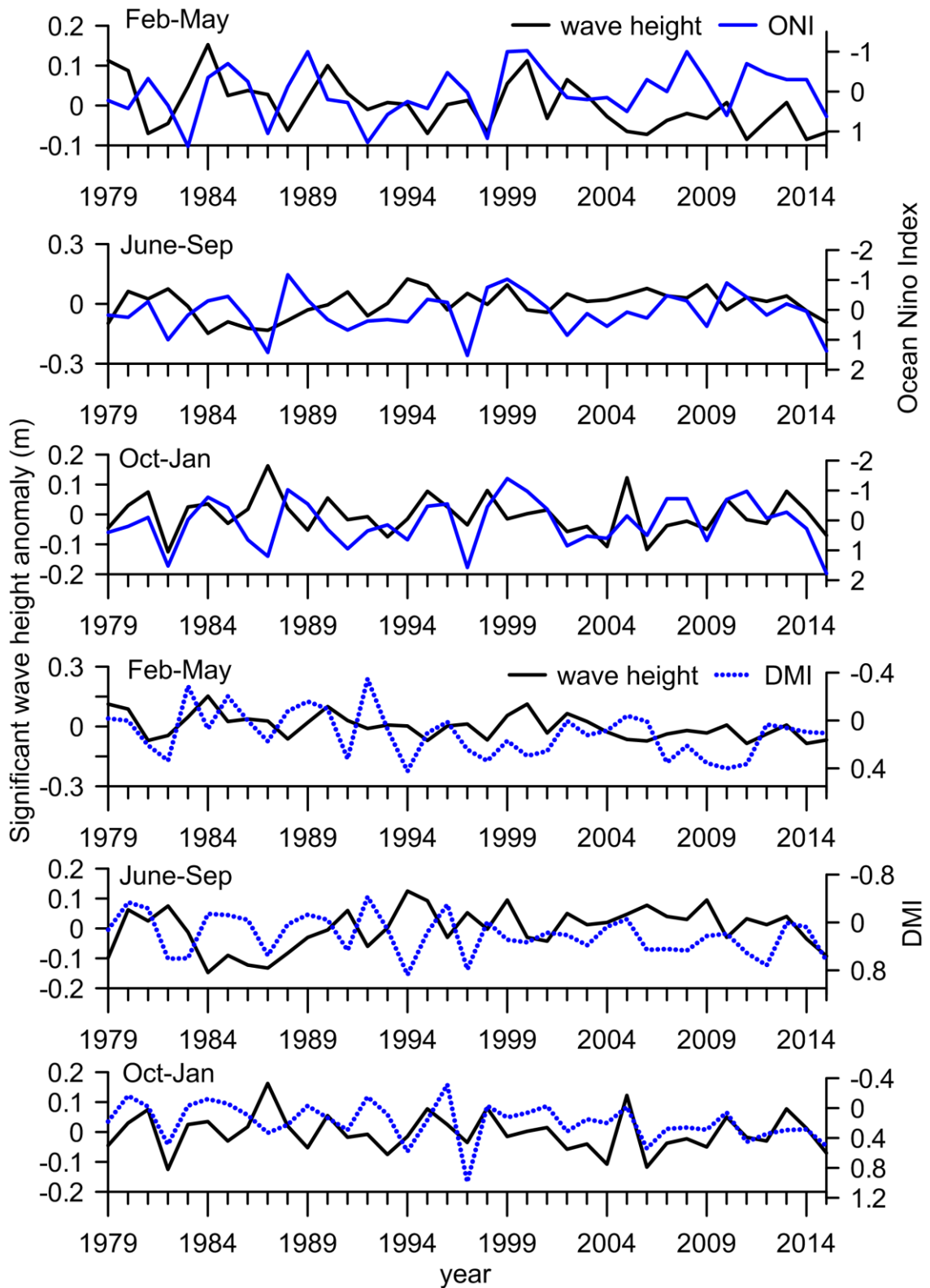


**Figure 18.** Time series of the seasonal anomaly significant wave height with the Ocean Niño Index and Dipole Mode Index